Palaeogeography, Palaeoclimatology, Palaeoecology 601 (2022) 111126

Contents lists available at ScienceDirect

Palaeogeography, Palaeoclimatology, Palaeoecology

journal homepage: www.elsevier.com/locate/palaeo

Differential enrichment mechanisms of organic matter in the Chang 7 Member mudstone and shale in Ordos Basin, China: Constraints from organic geochemistry and element geochemistry

Ruihui Zheng [a,b], Wenren Zeng [a,b], Zhipeng Li [a,b], Xue Chen [a,b], Kaixuan Man [a,b], Zhihuan Zhang [a,b,*], Guangli Wang [a,b], Shengbao Shi [a,b]

[a] College of Geosciences, China University of Petroleum, Beijing 102249, China
[b] State Key Laboratory of Petroleum Resources and Prospecting, China University of Petroleum, Beijing 102249, China

ARTICLE INFO

Editor: Dr. Shucheng Xie

Keywords:
Lacustrine shale and mudstone
Organic-matter enrichment
Biomarker
Trace element
Event deposition
Ordos Basin

ABSTRACT

Source rocks in the seventh member of the Upper Triassic Yanchang Formation (Chang 7 Member) are characterised by lacustrine organic-rich mudstone and organic-rich shale in the Ordos Basin. There are obvious differences in organic and inorganic geochemical characteristics between mudstone and shale in the Chang 7 Member, indicating that they are significantly different in genetic mechanism. Presently, the difference of organic-matter enrichment mechanism between shale and mudstone in the Chang 7 Member is still obscure. In this study, we explored the organic-matter accumulation mechanisms in the Chang 7 Member mudstone and shale by investigating their parent-rock properties, palaeoproductivity, palaeoenvironment and dilution conditions using biomarkers and elemental geochemical data. According to our analysis results, the mudstone and shale parent rocks are composed of sedimentary rock and granite. The material source of the mudstone was mainly from the south of the Ordos Basin, whilst the source of the shale was mainly from the south and northeast of the basin. The organic-matter enrichment of the shale was affected by high palaeoproductivity and anoxic environment conducive to the preservation of organic matter. The palaeoproductivity during the deposition of the mudstone was moderate, and the dilution caused by the high sedimentation rate was the main reason for its low abundance of organic matter. Affected by frequent volcanic activities, a grater algae bloom occurred in the process of the shale deposition, which made the palaeoproductivity during shale deposition higher than that of the mudstone deposition. In addition, the degradation of a large quantity of algae resulted in a reducing environment during shale deposition. Therefore, the high palaeoproductivity and anoxic preservation conditions resulted in large amounts of aquatic organisms in the shale, resulting in high organic-matter abundance in the shale. The palaeoclimate during mudstone deposition was warmer and wetter than during shale deposition, which was more conducive to parent-rock weathering and the transportation and deposition of terrigenous detritus. Therefore, the organic matter of mudstone is a mixture of terrestrial higher plants and aquatic organisms. However, the high input rate of terrigenous detritus caused the dilution of organic matter in the mudstone. The mudstone was mainly deposited under weakly oxidising to weakly reducing conditions. The moderate palaeoproductivity, oxygen-containing preservation conditions and dilution caused by the high sedimentation rate made the aquatic and terrestrial organic matter in the mudstone easily oxidised, degraded and diluted. Therefore, the differences of primary productivity and preservation conditions make the organic-matter abundance of the mudstone lower than that of the shale.

1. Introduction

Organic matter in the source rock is the material basis of oil and gas generation in sedimentary basins, and productivity, preservation conditions and sedimentation rate determine the enrichment degree of organic matter in source rocks. The productivity is mainly controlled by the parent-rock properties, climate and volcanism and hydrothermal activities (Zhang et al., 2017; Cao et al., 2020; Shen et al., 2021).

* Corresponding author at: College of Geosciences, China University of Petroleum, Beijing 102249, China.
E-mail address: zhangzh3996@vip.163.com (Z. Zhang).

https://doi.org/10.1016/j.palaeo.2022.111126
Received 4 January 2022; Received in revised form 16 June 2022; Accepted 18 June 2022
Available online 22 June 2022

Preservation conditions are mainly controlled by the redox environment and degradation in the post-deposition period (Lash and Blood, 2014; Zhang et al., 2017; Cao et al., 2020; Xu et al., 2022; Shi et al., 2022). The sedimentation rate is mainly controlled by the clastic influx rate (Chen et al., 2022). Three simple models of productivity, preservation and sedimentation rate were proposed to explain the organic-matter enrichment mechanism. Among them, the productivity model emphasises that the organic-matter enrichment is mainly controlled by high primary productivity caused by the eutrophication of water, and the influence of water redox conditions is limited (Pedersen and Calvert, 1990; Parrish, 1995; Gallego-Torres et al., 2007). The preservation model emphasises that organic-matter preservation is controlled by anoxic sedimentary bottom water environment, and low primary productivity can also form organic-rich sediments in anoxic environments, especially in the sulphide hydrostatic environments, such as those found in the Cretaceous marine anoxic event (Demaison and Moore, 1980; Canfield, 1989; Tyson and Pearson, 1991; Ingall et al., 1993; Arthur and Sageman, 1994; Mort et al., 2007). The sedimentation-rate model emphasises that the preservation of organic matter is controlled by the sedimentation-rate threshold. The amount of organic matter increases with the increase of sedimentation rate when the sedimentation rate is lower than the threshold value, and the amount of organic matter decreases with the increase of sedimentation rate when the rate exceeds the threshold value (Johnson Ibach, 1982; Murphy et al., 2000). However, different from some marine sedimentary basins, lacustrine sedimentary basins are easily affected by terrestrial organic-matter input, seasonal climate change and geological events (Chen et al., 2019; Xu et al., 2022). Therefore, the organic-matter enrichment is controlled by multiple factors in many marine and lacustrine sedimentary basins (Canfield, 1994; Crombez et al., 2017; Xu et al., 2022).

Various organic and inorganic geochemical parameters have been proposed to analyse the main controlling factors of organic-matter enrichment in source rocks. The enrichment of zinc (Zn), copper (Cu), molybdenum (Mo) and other essential nutrients and structural elements in sediments often indicates high primary productivity, and the depletion of these elements indicates low primary productivity (Ingall et al., 1993; Schenau et al., 2005; Tribovillard et al., 2006). The development of tuff and tuffaceous mudstone is related to volcanic activity (Zhang et al., 2017; Zhang et al., 2020), and the enrichment of Mo, Cu, uranium (U) and manganese (Mn) is related to hydrothermal activity (Murray, 1994; Zhang et al., 2017). Thus, development of tuff and tuffaceous mudstone and enrichment of Mo, Cu, U and Mn indicate the existence of geological events. Low strontium/copper (Sr/Cu) and gallium/rubidium (Ga/Rb) ratios indicate warm–humid palaeoclimatic conditions, whilst high ratios indicate arid–hot palaeoclimatic conditions (Lerman, 1978; Roy and Roser, 2013; Krzeszowska, 2019). A pristane/phytane (Pr/Ph) ratio < 1.0 usually indicates reducing conditions, whilst Pr/Ph > 2.0 usually indicates oxidising ones (Peters et al., 2005). In addition, the cross plots of Pr/nC_{17} and Ph/nC_{18} (Peters et al., 2005), Mo–U covariation (Algeo and Tribovillard, 2009) and the anomalies of cerium (Ce) and europium (Eu) (Trail et al., 2012) can also be used to reconstruct the palaeoredox conditions. High Gammacerane/C_{30} hopane (G/C_{30}H), C_{26}/C_{28}-20S- triaromatic steroid (C_{26}/C_{28}-20S-TAS) or strontium/barium (Sr/Ba) ratios correspond to saline water environments, whereas low ratios of these biomarkers and element parameters correspond to fresh-water environments (Peters et al., 2005; Meng et al., 2011; Wei and Algeo, 2020; Xu et al., 2022). The sedimentation rate can be analysed by the abundance and differentiation characteristics of rare-earth elements (REEs). High ratios of light REEs to heavy REEs (LREE/HREE) correspond to low sedimentation rates, whilst low ratios correspond to high sedimentation rates (Elderfield and Greaves, 1982). However, these organic and inorganic parameters have optimal application ranges and great uncertainty under complex geological conditions (Peters et al., 2005; Shi et al., 2022). Therefore, integrative applications of relevant parameters can obtain more reliable results.

Source rocks of the seventh member of the Yanchang Formation (Chang 7 Member) in the Ordos Basin are composed of mudstone and shale. Mudstone is characterised by dark-grey colour, high sand content (5%–20%), rough fractures and undeveloped lamellar structure; shale has the characteristics of black colour, low sand content (<5%), tidy fractures and well-developed lamellar structure (Lin et al., 2017; Liu et al., 2018; Fan et al., 2020; Zhao et al., 2020). The differences in petrological characteristics between mudstone and shale indicate that there are obvious differences in their genetic mechanism. So far, most studies on organic-matter enrichment of the Chang 7 Member source rocks have regarded the mudstone and shale as a whole and ignored their differences; or the studies only dealt with the shale and ignored the mudstone (Zhang et al., 2017; Yuan et al., 2017; Zhang et al., 2020; Zhang et al., 2021c,b; Shi et al., 2022). This leads to poor understanding of the organic-matter enrichment mechanism of mudstone and shale in the Chang 7 Member, which limits predictions of the effective source rock distribution areas.

In this work, biomarkers and trace elements were analysed to investigate the parent-rock properties and depositional environments of the Chang 7 mudstone and shale. The goal is to reveal the key factors controlling organic-matter enrichment in the mudstone and shale and establish their organic-matter enrichment models. This work will provide an important reference for predicting the occurrence of high-quality source rocks and for guiding the exploration and development of conventional and unconventional crude oil in the Upper Triassic of the Ordos Basin. Additionally, the results of this study will contribute to better understanding of the differences in geochemical characteristics between the mudstone and shale under the influence of geological events.

2. Geological setting

The Ordos Basin, located in northern central China, is a typical Mesozoic terrestrial lacustrine basin with an area of 37×10^4 km^2. It can be divided by structural characteristics into the Yimeng Uplift, Tianhuan Sag, Western Thrust Belt, Yishan Slope, Jinxi Fold Belt and Weibei Uplift (Fig. 1a). The basin experienced six major tectonic evolution stages since the Palaeoproterozoic Hutuo stratigraphy deposition (Yang et al., 2005). Among them, the collisional orogenic movement (Qinling Orogeny) between the North China Craton and the Yangtze Block resulted in intense tensional stress along the northeast–southwest direction, which controlled the evolution of the Ordos terrestrial lacustrine basin in the Mesozoic (Zhang et al., 2017). Therefore, the Upper Triassic Yanchang Formation recorded the whole depositional cycle of the Ordos lacustrine basin, and the maximum water area was approximately 1.0×10^5 km^2 in the Late Triassic (Yang, 2002). The Yanchang Formation can be divided by lithology into 10 members (Chang 10–Chang 1) from bottom to top, of which the Chang 7 Member is considered as the most important source rock in the Ordos Basin. The Chang 7 Member can be further divided into three layers (Chang 7^3, Chang 7^2 and Chang 7^1) from bottom to top (Fig. 1b). The lithology of the Chang 7 Member is mainly composed of sandstone, siltstone, mudstone and shale. The area of organic-rich mudstone and shale is 5.0×10^4 km^2, within which the mudstone was deposited in shallow to semi-deep lacustrine sub-facies, and shale was deposited in deep lacustrine sub-facies (Yang et al., 2010). The mudstone is mainly distributed in the Chang 7^1 and Chang 7^2 layers, and the shale mainly in the Chang 7^3 layer.

3. Samples and methods

3.1. Sample collection and pretreatment

In this study, 21 shale samples and 26 mudstone samples were selected from the Chang 7 Member for organic geochemical analysis. These samples came from 13 wells and 2 field outcrops, which are shown in Fig. 1a. Among these samples, 13 shales and 12 mudstones were selected for trace-element geochemical analysis.

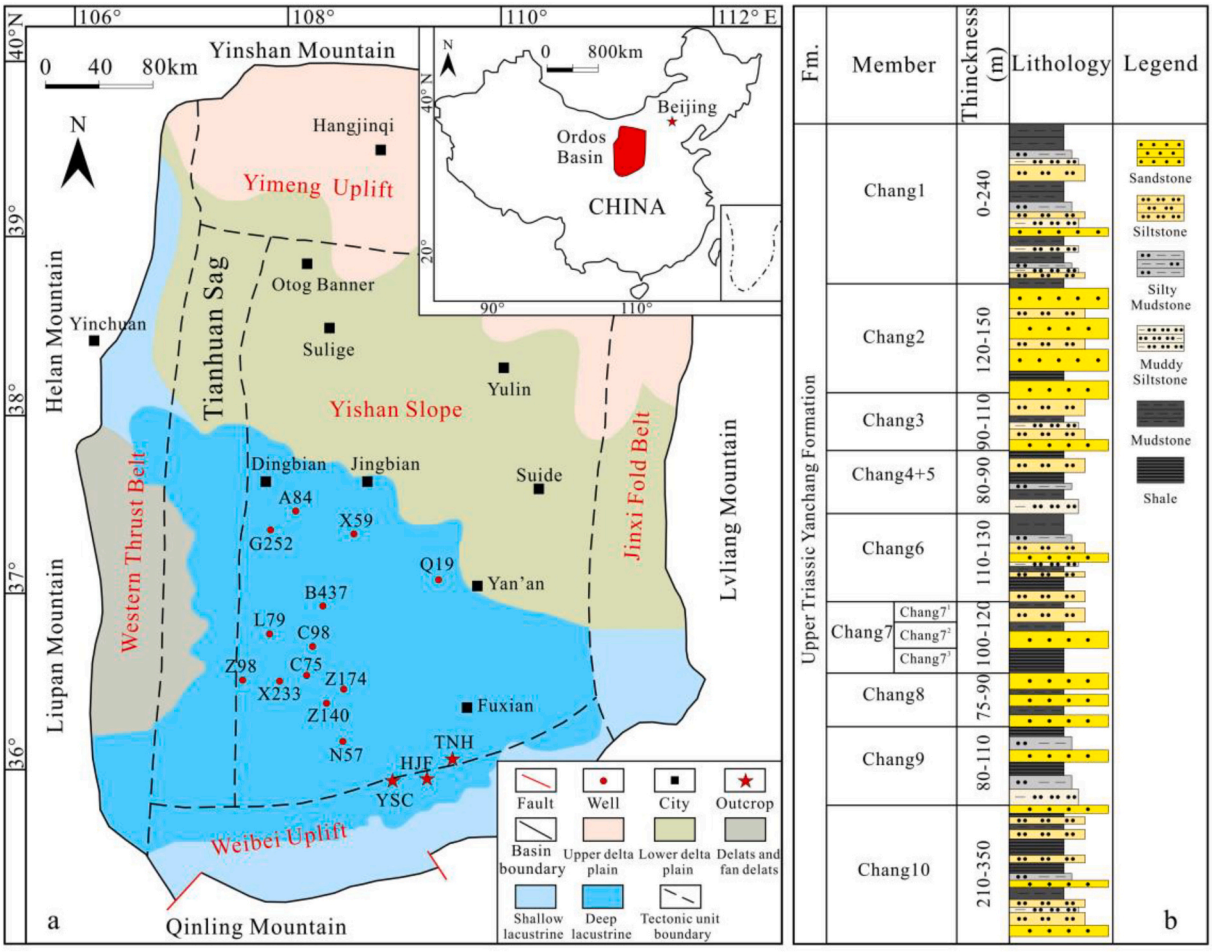

Fig. 1. (a) Division of structural units, location of wells and outcrops in the Ordos Basin (modified from Chen et al., 2017); (b) Stratigraphic division of the seventh member of Yanchang Formation (modified from Yang et al., 2010).

3.2. Total organic carbon content and Rock-Eval analysis

Total organic carbon (TOC) was analysed on the LECO CS 230 element analyser at the State Key Laboratory of Petroleum Resources and Prospecting in the China University of Petroleum–Beijing. Mudstone and shale of the Chang 7 Member were crushed and sieved to 100 mesh. A 100-mg quantity of mudstone and 10-mg shale for each sample were treated with 5% hydrochloric acid (HCl) at 80 °C to remove inorganic carbon from samples, then the samples were treated with distilled water for 24 h to clean the residual acid. Before analysis, the washed samples were dried in an oven at 70 °C for 8 h and iron powder and tungsten tin alloy were added as combustion improvers. The experimental materials are in line with the international quality standard system ISO9001 certification, and the instrument accuracy was ±0.5%.

The pyrolysis parameters of the shale and mudstone samples were analysed on the Rock-Eval II. The powder sample was first heated to 300 °C for 3 min to obtain free hydrocarbon (S_1), then continue heating to 600 °C at the rate of 25 °C/min to obtain pyrolysis hydrocarbon (S_2). According to above parameters, the hydrocarbon generation potential ($S_1 + S_2$) can be calculated.

3.3. Molecular biomarkers analysis

Based on the results of TOC analysis results, approximately 80-mg mudstone and approximately 50-mg shale were subjected to Soxhlet extraction using dichloromethane for 24 h to obtain soluble bitumen in the sample. After extraction, the deasphalted components was filtered from the extracts with petroleum ether, and the soluble part was further divided into saturated hydrocarbon, aromatic hydrocarbon and polar compounds by liquid–liquid phase separation (alumina:silica gel = 2:3). A 30-mL quantity of petroleum ether was used to separate the saturated hydrocarbon, a 20-mL mixture of dichloromethane and petroleum ether (V:V = 2:1) was used to separate aromatic hydrocarbon and 15-mL of dichloromethane was used to separate polar compounds.

The molecular biomarkers in the aliphatic fraction were analysed on an Agilent 6890 Gas Chromatograph (GC) equipped with a HP-5MS column (30-m × 0.25-mm i.d, with 0.25-μm film thickness) and linked with an Agilent 5975i Mass Spectrometer (MS). Helium was used as carrier gas. The initial temperature of the GC oven was set to 50 °C, then increased programmatically to 310 °C at the rate of 3 °C/min and kept isothermal for 25 min. The mass spectrometer was operated in FULL-SCAN mode. The electron ionization method was adopted (70 eV). The aromatic fraction was analysed following the same procedure as above, with the exception that the initial temperature of the GC oven was set to 80 °C, then increased programmatically to 310 °C at the rate of 3 °C/min and kept isothermal for 20 min.

3.4. Trace-element analysis

Trace-element analysis of mudstone and shale was completed at the Analytical Laboratory of the Beijing Research Institute of Uranium Geology, China. Mudstone and shale samples for trace-element analysis were crushed and sieved to 200 mesh, and these samples were dissolved in a mixture of hydrofluoric acid (HF, 30%) and nitric acid (HNO_3, 68%) at 190 °C for 24 h. Then, the solvent was removed by water-bath heating, and the treated sample was redissolved in 2 mL of 6 mol/L HNO_3 at

150 °C in capped Teflon bombs for 48 h. Finally, the residual solution was evaporated to near dryness again, and 1 mL of 6 mol/L HNO_3 was added. All samples were diluted for analysis. Trace elements were analysed on a Thermo Scientific Element inductively coupled plasma mass spectrometer (ICP-MS) according to the Chinese National Standard GB/T 14506.30–2010, and the detection limits for the elements ranged from 0.1 ppb to 9 ppb.

To evaluate the extent of enrichment for each trace element, we calculated their enrichment factor (EF) based on the formula: EF x = X_{sample}/ $X_{average\ shale}$, where the X_{sample} represents the abundance of trace element X in the samples, and $X_{average\ shale}$ represents the average abundance of trace element X in the shale composition of the Earth's crust (Turekian and Wedepohl, 1961). The studied element was considered enriched in the sample relative to the average shale if EF > 1, and depleted if EF < 1.

4. Results

4.1. Total organic carbon content and pyrolysis parameters

The TOC content is an important parameter for evaluating the abundance of organic matter in source rocks. In this study, the TOC content of mudstone and shale samples in the Chang 7 Member range from 0.51% to 7.35% (average 3.24%) and 6.13% to 39.39% (average 19.78%), respectively (Table 1). The $S_1 + S_2$ values of mudstone and shale in this member range from 0.54 mg/g to 20.28 mg/g (average 7.57 mg/g) and 6.45 mg/g to 174.30 mg/g (average 76.05 mg/g), respectively (Table 1). According to the evaluation criteria of organic-matter abundance given by Peters and Cassa (1994), the mudstones are evaluated as poor to good source rocks, and the shales correspond to good to excellent source rocks. Therefore, the hydrocarbon generation potential of the shale is higher than that of the mudstone.

Table 1
Geochemical and biomarker parameters of shale and mudstone samples from the Chang 7 Member, Ordos Basin.

Well/ Outcrop	Sample No	Lithology	TOC (%)	$S_1 + S_2$ (mg/g)	Pr/ Ph	Pr/ nC_{17}	Ph/ nC_{18}	G/ $C_{30}H$	Relative content (%)			Fla/ (Fla + Py)	C_{26}/ C_{28}-20S-TAS	Relative content (%)		
									C_{27}	C_{28}	C_{29}			DBT	DBF	F
A84	CQ-1	mudstone	5.18	20.28	1.41	0.25	0.18	0.15	28.25	20.27	51.47	0.15	0.35	26.73	29.88	43.39
X59	CQ-2	mudstone	4.76	16.64	1.56	0.22	0.14	0.20	39.53	19.51	40.96	0.13	0.29	47.98	29.67	22.35
Q19	CQ-3	mudstone	4.94	14.58	1.56	0.18	0.11	0.12	40.34	23.24	36.42	0.15	0.38	24.36	11.69	63.95
C98	CQ-4	mudstone	1.98	4.85	1.12	0.27	0.25	0.20	26.40	32.87	40.73	0.23	0.54	61.68	23.89	14.43
C75	CQ-5	mudstone	3.42	4.30	1.02	0.23	0.20	0.09	32.61	15.68	51.71	0.10	0.49	69.25	7.14	23.61
C75	CQ-6	mudstone	7.19	19.68	1.11	0.20	0.19	0.20	39.89	24.61	35.50	0.08	0.36	62.28	18.68	19.04
C75	CQ-7	mudstone	0.52	0.54	1.25	0.42	0.30	0.17	26.31	14.69	59.00	0.18	0.38	48.06	19.84	32.10
C75	CQ-8	mudstone	0.70	1.14	1.18	0.42	0.32	0.16	19.09	28.55	52.35	0.19	0.24	55.30	11.52	33.18
C75	CQ-9	mudstone	2.42	1.48	1.14	0.31	0.27	0.24	21.43	29.44	49.13	0.13	0.39	73.64	16.21	10.15
C75	CQ-10	mudstone	0.64	1.38	0.91	0.41	0.33	0.13	21.27	28.28	50.45	0.21	0.27	56.67	7.82	35.51
C75	CQ-11	mudstone	0.57	0.54	1.23	0.49	0.37	0.19	35.38	21.50	43.13	0.24	0.62	52.88	25.42	21.70
C75	CQ-12	mudstone	0.51	0.56	1.28	0.43	0.35	0.18	37.53	18.88	43.58	0.24	0.45	82.49	5.31	12.20
C75	CQ-13	mudstone	0.70	0.65	1.28	0.53	0.39	0.14	17.50	28.26	54.24	0.26	0.34	72.78	1.38	25.84
C75	CQ-14	mudstone	3.47	4.30	0.99	0.22	0.23	0.12	25.26	33.01	41.73	0.12	0.44	54.50	17.38	28.12
C75	CQ-15	mudstone	4.19	5.53	1.11	0.29	0.29	0.13	29.70	33.15	37.15	0.10	0.51	66.11	17.28	28.12
C75	CQ-16	mudstone	1.97	3.04	0.72	0.33	0.29	0.14	44.31	20.69	35.00	0.18	0.51	78.89	7.35	13.76
Z98	CQ-17	mudstone	6.05	16.63	1.29	0.24	0.20	0.09	25.83	27.96	46.21	0.07	0.25	56.24	34.33	9.44
Z98	CQ-18	mudstone	6.89	19.96	1.26	0.23	0.19	0.09	29.48	27.49	43.03	0.07	0.27	62.49	28.85	8.65
Z98	CQ-19	mudstone	5.08	17.04	1.32	0.24	0.20	0.09	28.08	28.16	43.76	0.18	0.24	65.54	26.48	7.98
X233	CQ-20	mudstone	1.61	4.08	1.09	0.33	0.31	0.12	43.47	19.46	37.06	0.16	0.35	66.80	20.36	12.84
X233	CQ-21	mudstone	5.34	14.46	0.98	0.29	0.31	0.11	23.99	30.07	45.94	0.07	0.36	58.97	12.64	28.39
X233	CQ-22	mudstone	2.54	9.10	0.88	0.48	0.50	0.09	39.82	24.14	36.04	0.11	0.30	52.85	32.62	14.53
X233	CQ-23	mudstone	1.87	6.05	1.18	0.30	0.26	0.20	43.36	19.76	36.89	0.18	0.37	40.59	33.48	25.93
Z174	CQ-24	mudstone	3.01	1.43	0.97	0.55	0.47	0.10	24.29	28.60	47.10	0.20	0.49	82.15	3.98	13.87
Z174	CQ-25	mudstone	7.35	3.75	1.00	0.22	0.23	0.17	45.14	22.65	32.21	0.10	0.46	30.86	16.33	52.81
N57	CQ-26	mudstone	1.46	4.92	0.82	0.37	0.46	0.11	36.66	28.27	35.06	0.25	0.30	24.82	31.94	43.24
G252	CQ-27	shale	13.68	54.50	0.79	0.14	0.20	0.06	43.62	23.28	33.10	0.05	0.33	86.18	4.69	9.13
B437	CQ-28	shale	33.17	130.36	0.69	0.14	0.13	0.07	38.65	29.14	32.21	0.05	0.32	93.75	2.26	3.99
L79	CQ-29	shale	6.34	23.14	0.85	0.38	0.54	0.07	45.60	25.49	28.91	0.15	0.46	81.44	7.98	10.58
L79	CQ-30	shale	21.11	83.38	0.74	0.11	0.17	0.02	59.71	16.73	23.56	0.08	0.39	79.56	10.31	10.13
C98	CQ-31	shale	10.68	21.27	0.75	0.34	0.36	0.11	38.08	30.86	31.06	0.07	0.40	81.68	15.30	3.02
C75	CQ-32	shale	8.83	14.76	0.83	0.44	0.32	0.09	55.31	15.95	28.74	0.19	0.38	95.49	1.37	3.14
C75	CQ-33	shale	6.69	11.88	0.93	0.24	0.26	0.09	39.30	27.69	33.01	0.11	0.45	54.50	17.38	28.12
C75	CQ-34	shale	6.14	10.09	0.97	0.32	0.33	0.09	37.55	25.88	36.57	0.09	0.52	63.91	21.45	14.65
C75	CQ-35	shale	6.12	6.45	0.87	0.30	0.30	0.09	43.85	22.68	33.47	0.12	0.46	89.69	5.83	4.48
Z140	CQ-36	shale	13.16	76.74	0.95	0.29	0.36	0.08	37.16	30.21	32.62	0.07	0.48	70.34	19.61	10.04
TNH	CQ-37	shale	35.59	150.38	0.65	0.40	0.44	0.03	31.41	31.85	36.74	0.09	0.33	92.41	2.91	4.67
TNH	CQ-38	shale	19.86	71.56	0.80	0.47	0.54	0.04	27.82	31.12	41.06	0.07	0.30	77.37	17.23	5.40
TNH	CQ-39	shale	18.44	83.37	0.79	0.48	0.62	0.04	26.11	31.86	41.02	0.04	0.29	71.45	25.67	2.89
TNH	CQ-40	shale	39.39	174.30	0.51	0.44	0.55	0.03	26.47	31.11	42.42	0.08	0.28	80.34	12.82	6.83
TNH	CQ-41	shale	16.76	75.13	0.83	0.62	0.69	0.05	24.04	32.39	43.56	0.06	0.28	81.13	14.46	4.41
TNH	CQ-42	shale	23.42	90.23	0.86	0.37	0.45	0.04	26.38	32.05	43.56	0.06	0.29	76.03	20.75	3.22
TNH	CQ-43	shale	27.24	105.55	0.82	0.44	0.49	0.04	26.67	31.32	42.02	0.06	0.30	85.26	9.90	4.84
TNH	CQ-44	shale	18.47	61.81	0.83	0.31	0.41	0.04	27.93	30.05	42.02	0.07	0.30	70.29	26.48	3.23
TNH	CQ-45	shale	29.71	129.69	0.72	0.33	0.42	0.03	27.21	32.23	40.56	0.06	0.32	74.54	22.89	2.57
HJF	CQ-46	shale	32.84	135.09	0.48	0.26	0.45	0.04	29.09	29.77	41.14	0.09	0.30	62.10	28.02	9.88
HJF	CQ-47	shale	27.73	87.47	0.53	0.26	0.45	0.04	29.01	29.57	41.42	0.08	0.31	62.07	25.29	12.65

Pr: pristane, Ph: phytane, G: gammacerane, H: hopane, Fla.: fluoranthene, Py: pyrene, TAS: triaromatic steroid, DBT: dibenzothiophene, DBF: dibenzofuran, F: Fluorene.

4.2. Molecular geochemistry

4.2.1. Saturated hydrocarbon compounds

The biomarker compound distribution characteristics of the saturated hydrocarbons in the Chang 7 Member mudstone and shale are shown in Fig. 2a–f. The n-alkanes of shale and mudstone in this member are characterised by unimodal distributions (Fig. 2a and b), and Pr and Ph are the main acyclic isoprenoids in the mudstone and shale samples. The Pr/Ph, Pr/nC_{17} and Ph/nC_{18} ratios are shown in Table 1.

For similar maturity, the contents of tricyclic terpanes and pregnanes in shales are higher than those in mudstones, whilst the concentrations of C_{30}-rearranged hopane in mudstones are higher than those in shales (Fig. 2c–f). The abundance of 18α(H),21β(H)-22,29,30-trisnorneohopane (Ts) is greater than that of 17α(H),21β(H)-22,29,30-trisnorhopane (Tm) in the samples. In addition, low concentrations of gammacerane have been detected in shales and mudstones.

4.2.2. Aromatic hydrocarbon compounds

The typical mass fragmentograms of the aromatic fractions from the Chang 7 Member shale and mudstone are shown in Fig. 2g and h, respectively. Polycyclic compounds such as phenanthrene (P), fluoranthene (Fla) and pyrene (Py) have been detected in these shales and mudstones, and the Fla./(Fla + Py) ratio is shown in Table 1. Dibenzothiophene (DBT), dibenzofuran (BDF) and fluorene (F) also have been detected in these samples, and their relative contents are shown in Table 1. In addition, different contents of triaromatic steroids are detected in the samples, and the ratios of C_{26}/C_{28}-20S- TAS are shown in Table 1.

4.3. Element geochemistry

The trace elements raw data and related parameters for the Chang 7 Member mudstone and shale are listed in Table 2 and Table 3. Compared to the average content of shale element composition in the Earth's crust (Turekian and Wedepohl, 1961), the analysed mudstone samples are enriched in scandium (Sc), manganese (Mn), copper (Cu), gallium (Ga), rubidium (Rb), yttrium (Y), niobium (Nb), zirconium (Zr), molybdenum (Mo), barium (Ba), lead (Pb), thorium (Th) and uranium (U), whilst the shale samples are enriched in vanadium (V), Cu, Mo, Pb and U (Fig. 3). Cu, Mo and U were more enriched in the shales (Cu_{EF}: 0.83–3.40, average (avg.) 2.14; Mo_{EF}: 0.50–51.31, avg. 29.99; U_{EF}: 0.97–23.92, avg. 10.22) compared to the mudstones (Cu_{EF}: 0.66–2.36, avg. 1.19; Mo_{EF}: 0.38–28.92, avg. 6.81; U_{EF}: 0.92–8.08, avg. 3.09) (Table 3 and Fig. 3). In addition, the REE contents in the mudstones are higher than those in the shales (Fig. 3).

5. Discussions

5.1. Main factors affecting organic matter enrichment

5.1.1. Parent-rock properties

The chemical composition of terrestrial sediments is a comprehensive reflection of the results of parent-rock weathering, transportation and diagenesis, and the REEs changed little in this process (Bhatia and Taylor, 1981; Armstrong-Altrin et al., 2015). Therefore, the REEs can provide important parent-rock lithological characteristics. The La/Yb ratios of the Chang 7 Member mudstone and shale samples range from 8.0 to 16.5 and from 9.6 to 18.1, respectively (Table 2). In the diagram of La/Yb vs. ∑REEs proposed by Allègre and Minster (1978), the Chang 7 Member mudstone and shale samples are located in the overlapping zone between sedimentary rock and granite (Fig. 4a), indicating that their parent-rock properties are basically the same. Moreover, REE distribution patterns are considered to be a vital tracer for parent rocks (Meclennan, 1993). The REE distribution pattern in the Chang 7 Member mudstone is similar to that of magmatic rocks of the Qinling Orogen (Fig. 4b), whilst that of the Chang 7 Member shale is similar to that of the magmatic rocks of the Qinling Orogen and basement rocks in the northeastern Ordos Basin (Fig. 4c) (Luo et al., 2007; Wang et al., 2013). Therefore, the parent-rock properties of the mudstone and shale are basically the same, both of which are the mixture of sedimentary rock and granite. However, the mudstone and shale parent rocks originated from different areas. The provenance of the mudstone was from the southern Ordos Basin, whilst the provenance of the shale was from the southern and northeastern Ordos Basin.

5.1.2. Palaeoproductivity

5.1.2.1. Palaeoclimate. Fla. and Py are considered to be the products of original organic matter and biomass combustion, and biomass combustion generally occurs in the arid climates (Sicre et al., 1987). Therefore, the ratio of Fla./(Fla + Py) can be used as an indicator for biomass combustion and arid climates (Yunker et al., 2011). Fla./(Fla + Py) values <0.4 indicate that Fla. and Py originate from the diagenetic transformation of organic matter, whilst Fla./(Fla + Py) values >0.5 indicate Fla. and Py originate from biomass combustion. Fla./(Fla + Py) values of 0.4–0.5 indicate mixed sources (Yunker et al., 2011). The Fla./(Fla + Py) ratios of the Chang 7 Member shale and mudstone vary from 0.04 to 0.19 and from 0.07 to 0.26 (Table 1), respectively. The Fla./(Fla + Py) ratios of mudstone and shale are low, indicating that the climate was humid during deposition.

The Sr/Cu ratio is an important palaeoclimate indicator; a low Sr/Cu ratio (1.3–5.0) reflects warm–humid climate conditions, a moderate ratio (5.0–10.0) reflects semi-arid–humid climate conditions and a high one (> 10.0) reflects arid–hot climate conditions (Lerman, 1978). The Sr/Cu ratios of the Chang 7 Member shales range from 0.55 to 2.92 (Table 3), with an average of 1.44. The Sr/Cu ratios of the Chang 7 Member mudstones range from 1.03 to 4.57 (Table 3), with an average of 2.98. These Sr/Cu ratios suggest that the shale and mudstone were deposited under warm–humid climate conditions.

The increase of Ga/Rb values corresponds to the increase of temperature and the decrease of humidity (Roy and Roser, 2013). The Ga/Rb ratios of the Chang 7 Member shales range from 0.08 to 0.28 (Table 3), with an average of 0.17, and the ratios of the mudstones range from 0.10 to 0.16 (Table 3), averaging 0.13. The relatively low Ga/Rb ratio of the Chang 7 Member mudstone indicates that the palaeoclimate during mudstone deposition was warmer and wetter than that during shale deposition.

Generally, an arid climate limits the large-scale growth of organisms (Xu et al., 2022). The Fla./(Fla + Py) vs. TOC and Sr/Cu vs. TOC plots show obvious negative correlations with R^2 values of 0.6257 and 0.7015, respectively, in the Chang 7 Member mudstone, indicating that the palaeoclimate had a strong effect on the organic-matter enrichment in mudstone (Fig. 5a1 and 5a2). The Fla./(Fla + Py) vs. TOC and Sr/Cu vs. TOC plots show slight negative correlations with R^2 values of 0.1929 and 0.4893, respectively, in the Chang 7 Member shale, indicating that the effect of palaeoclimate on the organic-matter enrichment of shale was weak (Fig. 5b1 and 5b2).

Consequently, the palaeoclimate during mudstone deposition was warmer and wetter than that during shale deposition and was more conducive to the supply of terrigenous organic matter. The relationship between palaeoclimate and TOC shows that terrestrial organisms have a strongly positive impact on the abundance of organic matter in mudstone, but their impact on the abundance of organic matter in shale is limited.

5.1.2.2. Palaeoproductivity. The primary productivity of the lake during sedimentation plays a vital role in the organic-matter enrichment (Zhang et al., 2017). Generally, the Cu enrichment rate in the sediments corresponds to the productivity of the lake, therefore, its content can be used as an effective index to evaluate the palaeoproductivity of the lake (Tribovillard et al., 2004, 2006; Schoepfer et al., 2016). A higher Cu

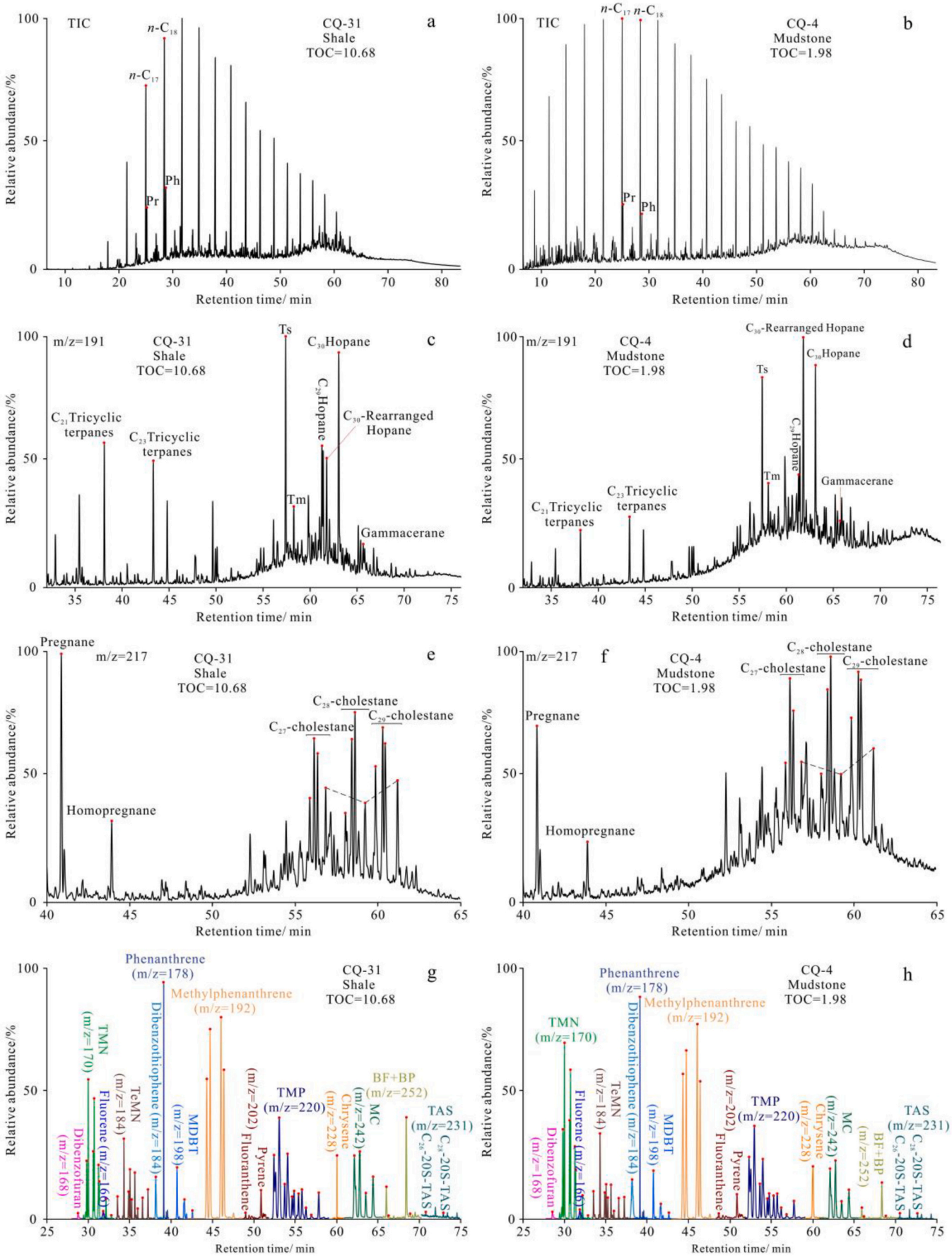

(caption on next page)

Fig. 2. Comparison of saturated and aromatic compounds between shale and mudstone in seventh member of Yanchang Formation, Ordos Basin (a and b, Total ion chromatograms (TIC) of saturated hydrocarbon factions; c and d, *m/z* = 191 gas chromatographic mass spectrometry diagrams (terpanes); e and f, m/z = 217 gas chromatographic mass spectrometry diagrams (steranes); g and h, Total ion chromatograms (TIC) of aromatic hydrocarbon factions). Note: TMN: Trimethyl naphthalene; TeMN: Tetramethyl naphthalene; MDBT: Methyl dibenzothiophene; TMP: Trimethyl phenanthrene; MC: Methyl Chrysene; BF: Benzofluoranthene; BP: Benzopyrene; TAS: Triaromatic steroid.

content corresponds to higher palaeoproductivity. In the Chang 7 Member mudstone samples, the contents and enrichment factors of Cu range from 29.9 ppm to 106.1 ppm and from 0.66 to 2.36 (Table 3), respectively, and the Cu contents and enrichment factors for shales range from 37.3 ppm to 162.9 ppm and from 0.83 to 3.62, respectively (Table 3). The contents and enrichment factors of Cu in shales are higher than those in mudstones, indicating that the palaeoproductivity of the lake during shale deposition is higher than that during mudstone deposition.

As shown in Fig. 6, the Cu vs. TOC and Cu_{EF} vs. TOC show positive correlations for the Chang 7 Member mudstones, with an R^2 of 0.8596 (Fig. 6a1 and 6a2) and for the shales with an R^2 of 0.541 (Fig. 6b1 and 6b2). The results indicate that the palaeoproductivity of the water column has a strong impact on organic-matter enrichment during mudstone deposition, whilst palaeoproductivity has a relatively weak impact on organic-matter enrichment during shale deposition.

5.1.2.3. Event deposition. Geological events often break the original ecosystem balance and affect the enrichment of organic matter. For example, volcanic eruptions will cause large-scale organism death, but volcanic ash deposition will make the water eutrophic and improve the productivity (Langmann et al., 2010; Zhang et al., 2017; Li et al., 2020; Zheng et al., 2022). The existence of volcanic eruption events in the Triassic Chang 7 shale sedimentary period has been confirmed by element and mineral assemblage characteristics (Qiu et al., 2015; He et al., 2016; Liao et al., 2019; Zhang et al., 2020). In the Yishicun (YSC) outcrop of the Chang 7 Member, laminar tuff and tuffaceous mudstone are interbedded with shale (Fig. 7a). In the core photomicrographs of the Chang 7 Member shales, the laminations are composed of organic-matter, clay and tuff layers (Fig. 7b). In the core photomicrographs of the Chang 7 Member mudstones, the laminations are mainly composed of organic-matter debris and clay layer (Fig. 7c). These results show that the organic-matter enrichment of shale is closely related to volcanic activity in the Triassic Chang 7 period.

Hydrothermal activity causes Mo, Cu, U and Mn enrichment in sedimentary rocks and this enrichment can be used to indicate the existence of hydrothermal sedimentation (Murray, 1994; Zhang et al., 2017). In this study, Cu (Cu_{EF}: 0.83–3.40, avg. 2.14), Mo (Mo_{EF}: 0.50–51.31, avg. 29.99) and U (U_{EF}: 0.97–23.92, avg. 10.22) are enriched in shale, whilst Mn (Mn_{EF}: 0.13–5.55, avg. 1.25), Cu (Cu_{EF}: 0.66–2.36, avg. 1.19), Mo (Mo_{EF}: 0.38–28.92, avg. 6.81) and U (U_{EF}: 0.92–8.08, avg. 3.09) are enriched in mudstone (Fig. 3, Table 3). These results indicate that hydrothermal activity occurred during deposition of the Chang 7 Member shale and mudstone and that the hydrothermal activity was more frequent during shale deposition. The depletion of Mn (Mn_{EF}: 0.07–1.04, avg. 0.26; Fig. 3, Table 3) in the Chang 7 Member shale is related to its deposition under a reducing sedimentary environment, the Mn oxides are transformed into soluble Mn and transferred to the sedimentary water under reducing conditions (Yu et al., 2016).

Previous studies found that the relationships among Ce anomalies, neodymium (Nd) concentrations and yttrium (Y) anomalies can be used to effectively distinguish types of sediments without considering their mineral composition (Bau et al., 2014; Afify et al., 2018; Zhang et al., 2020) (Fig. 8a and b). In the Nd–δCe* discriminant diagram, the mudstone samples of the Chang 7 Member fall into the diagenetic zone, whilst the shale samples fall into the hydrothermal and diagenetic zones (Fig. 8a). In the Y_{SN}/Ho_{SN} - δCe* (the subscript SN represents the shale of PAAS; Mclennan, 1989) discriminant diagram, the mudstone samples fall into the hydrothermal and diagenetic zone, whilst the shale samples fall into the hydrothermal zone (Fig. 8b). These results demonstrate that the depositional period of mudstone and shale in the Chang 7 Member was controlled by both hydrothermal activity and diagenesis, and the hydrothermal activity during shale deposition is stronger than that during mudstone deposition. In terms of the U–Th relationship, the U/Th ratios of normal sedimentary rocks are <1.0, whilst those of hydrothermal sedimentary rocks are >1.0 (Rona and Lowell, 1978). In the Log ($Th/10^{-6}$)- Log ($U/10^{-6}$) discriminant diagram, most of the mudstone and shale samples fall into the U/Th >1.0 zone (Fig. 8c). The results further confirm that the deposition of the Chang 7 Member mudstone and shale was controlled by hydrothermal activity.

In summary, there were obvious volcanic and hydrothermal events that affected the Chang 7 Member shale deposition. The volcanic activity was weak during the Chang 7 Member mudstone deposition, and the deposition process was affected by hydrothermal events. Therefore, water eutrophication caused by event deposition is the main reason for the difference of primary productivity between the mudstone and shale. In addition, the differences of parent-rock properties can lead to higher primary productivity during shale deposition than during mudstone formation (Cao et al., 2020).

5.1.3. Preservation conditions

5.1.3.1. Redox conditions. Biomarker parameters (e.g. Pr/Ph, Pr/nC_{17} vs. Ph/nC_{18}) are often used to indicate redox conditions of the water column. The Pr/Ph ratios of <0.5, 0.5–1.0, 1.0–2.0 and > 2.0 correspond to anoxic, reducing, weakly reducing to weakly oxidising and oxidising conditions, respectively (ten Haven et al., 1987; Peters and Moldowan, 1993). The Pr/Ph ratios of the Chang 7 Member shale and mudstone samples range from 0.48 to 0.97 and from 0.72 to 1.56, respectively (Table 1, Fig. 9a). The Pr/Ph ratios obtained indicate reducing conditions of the water during shale deposition and reducing to weakly oxidising conditions during mudstone deposition. Additionally, cross plots of Pr/nC_{17} vs. Ph/nC_{18} can be used to determine redox conditions and organic-matter sources (Sarki Yandoka et al., 2015; Qiao et al., 2021). The Pr/nC_{17} and Ph/nC_{18} ratios of the Chang 7 Member shales range from 0.11 to 0.62 and from 0.13 to 0.69, respectively (Table 1). The results show that the shale was mainly deposited under reducing conditions and the organic matter was mainly composed of algae (Fig. 9b). The Pr/nC_{17} and Ph/nC_{18} ratios of the Chang 7 Member mudstones range from 0.18 to 0.55 and from 0.11 to 0.50, respectively (Table 1). The results indicate that the mudstone was mainly deposited under suboxic conditions and the organic matter was a mixture of algae and higher plants (Fig. 9b). The ternary diagram of C_{27}–C_{28}–C_{29} ααα*R* steranes further proves that the organic matter of shale is mainly composed of algae, whilst that of mudstone is a mixture of algae and higher plants (Fig. 9c). Generally, the DBT content is higher under reducing conditions, whilst the content of DBF is higher under oxidising conditions. Therefore, the relative concentrations of DBT, DBF and F can be used to identify the redox conditions (Hughes et al., 1995; Li et al., 2013). The DBT concentration of the Chang 7 Member shale is higher than that of the mudstone (Fig. 9d), indicating that the shale is deposited in a more reducing environment than the mudstone.

The Mo and U concentrations in sediments are relevant to the redox conditions under which sediments are deposited; thus, the Mo_{EF}, U_{EF} and δU can be used as indicators to evaluate the redox conditions of the palaeowater column (Akinlua et al., 2010; Arsairai et al., 2016; Zhang et al., 2020). The values of Mo_{EF} and U_{EF} in the Chang 7 Member mudstone range from 0.38 to 28.92 and from 0.92 to 8.08, respectively

Table 2
The rare earth element composition of mudstone and shale samples from the Chang 7 Member, Ordos Basin.

Sample No	Lithology	Rare earth element (ppm)															Parameters				
		La	Ce	Pr	Nd	Sm	Eu	Gd	Tb	Dy	Ho	Er	Tm	Lu	Yb	∑REE	LREEs/HREEs	La/Yb	$(La/Yb)_N$	δCe*	Y_{SN}/Ho_{SN}
CQ-5	mudstone	50.6	108.9	12.0	43.4	7.0	1.5	5.8	0.9	5.1	1.0	3.1	0.5	0.5	3.4	243.9	10.96	14.91	1.47	1.02	1.07
CQ-6	mudstone	38.1	69.6	9.0	34.0	6.2	1.4	5.2	0.9	4.8	0.9	2.6	0.4	0.4	4.8	178.6	7.19	13.77	0.79	0.87	1.11
CQ-7	mudstone	48.3	94.1	11.5	42.6	7.1	1.7	6.1	1.0	5.7	1.2	3.4	0.5	0.5	3.6	227.3	9.36	13.58	1.34	0.92	1.03
CQ-8	mudstone	48.2	94.8	11.8	42.9	7.2	1.6	5.8	0.9	4.9	1.0	2.7	0.4	0.4	2.9	225.5	10.87	16.51	1.62	0.92	1.01
CQ-9	mudstone	31.4	57.4	7.3	27.4	4.4	1.0	3.8	0.6	3.4	0.7	2.0	0.3	0.3	2.1	142.0	9.85	15.26	1.50	0.87	1.20
CQ-10	mudstone	50.2	95.1	11.8	42.7	7.0	1.6	5.9	1.0	5.4	1.1	3.0	0.5	0.5	3.2	229.0	10.14	15.83	1.56	0.90	1.04
CQ-11	mudstone	54.2	103.6	12.5	45.8	7.4	1.6	6.2	1.0	5.6	1.1	3.2	0.5	0.5	3.4	246.7	10.44	15.86	1.56	0.92	1.07
CQ-12	mudstone	46.5	90.8	11.1	39.9	6.5	1.5	5.6	0.9	5.0	1.0	2.9	0.5	0.4	2.9	215.4	10.21	15.93	1.57	0.92	1.06
CQ-13	mudstone	45.1	88.9	10.9	39.7	6.5	1.5	5.4	0.9	4.6	0.9	2.5	0.4	0.4	2.8	210.4	10.84	15.96	1.57	0.92	1.05
CQ-14	mudstone	37.3	66.9	8.7	33.3	6.2	1.5	5.9	1.0	5.8	1.3	3.9	0.7	0.7	4.4	177.6	6.47	8.42	0.83	0.86	1.29
CQ-15	mudstone	28.8	54.6	6.9	25.3	4.7	1.3	3.9	0.7	3.4	0.7	1.9	0.3	0.3	2.2	134.9	9.07	13.36	1.31	0.89	1.08
CQ-16	mudstone	18.4	32.4	4.5	18.0	3.4	0.8	3.1	0.5	2.7	0.5	1.5	0.2	0.2	1.5	88.0	7.48	12.18	1.20	0.82	1.25
CQ-32	shale	47.3	93.6	11.9	43.3	6.6	1.4	5.1	0.8	4.3	0.8	2.4	0.4	0.4	2.8	221.1	11.93	16.77	1.65	0.91	1.08
CQ-33	shale	38.3	72.7	9.2	34.3	5.8	1.3	5.1	0.9	4.7	0.9	2.6	0.4	0.4	2.8	179.5	9.08	13.66	1.34	0.89	1.15
CQ-34	shale	34.1	63.1	7.9	28.5	4.6	1.0	3.9	0.6	3.6	0.8	2.4	0.4	0.5	3.1	154.7	9.11	11.02	1.08	0.88	1.20
CQ-35	shale	20.9	42.2	5.3	21.0	3.8	0.9	3.3	0.5	2.6	0.5	1.2	0.2	0.2	1.2	103.6	9.82	18.12	1.78	0.93	0.98
CQ-37	shale	22.0	37.3	4.8	18.1	3.7	0.9	3.0	0.5	2.4	0.5	1.3	0.2	0.2	1.4	96.3	9.06	16.22	1.60	0.84	0.95
CQ-38	shale	31.2	61.5	6.8	24.1	4.0	0.9	3.3	0.5	2.5	0.5	1.5	0.3	0.3	1.6	138.9	12.32	19.00	1.87	0.98	1.01
CQ-39	shale	27.6	51.1	6.5	24.6	4.6	1.0	4.0	0.6	3.4	0.7	2.1	0.3	0.3	2.1	129.0	8.46	13.19	1.30	0.88	1.12
CQ-40	shale	25.6	47.9	5.8	20.4	3.6	0.8	2.9	0.4	2.3	0.4	1.3	0.2	0.2	1.4	113.3	11.22	17.90	1.76	0.91	1.09
CQ-41	shale	10.1	16.1	2.4	8.5	1.8	0.5	1.5	0.2	1.4	0.3	0.9	0.2	0.2	1.0	45.1	6.95	10.08	0.99	0.76	1.00
CQ-42	shale	43.5	79.2	10.1	38.2	6.9	1.5	5.8	0.9	5.0	1.0	2.8	0.5	0.4	2.8	198.7	9.31	15.68	1.54	0.87	1.02
CQ-43	shale	41.0	76.8	9.5	33.3	5.5	1.0	4.6	0.7	4.0	0.8	2.3	0.4	0.4	2.3	182.5	10.78	18.13	1.78	0.90	0.99
CQ-44	shale	25.5	44.0	5.8	22.1	4.4	1.1	3.7	0.6	3.1	0.6	1.7	0.3	0.3	1.7	114.7	8.72	15.31	1.51	0.83	1.02
CQ-45	shale	31.3	55.0	7.4	30.1	5.5	1.4	5.2	0.9	4.9	1.1	3.1	0.5	0.5	3.2	150.2	6.75	9.64	0.95	0.83	1.23

N: the North American Shale Composite, Gromet et al., 1984; SN: the shale of PAAS, Mclennan, 1989.

Table 3
Trace element composition of mudstone and shale samples from the Chang 7 Member, Ordos Basin.

Sample No	Lithology	Trace element content (ppm)																			
		Li	Be	Sc	V	Cr	Mn	Co	Ni	Cu	Zn	Ga	Rb	Sr	Y	Nb	Zr	Mo	Ba	Pb	Th	U
CQ-5	mudstone	41.4	3.7	16.3	123.4	96.2	279.1	26.6	47.4	52.0	72.6	23.6	146.9	144.1	29.2	17.6	314.5	1.7	646.4	61.9	20.1	4.9
CQ-6	mudstone	45.2	2.9	17.4	158.3	64.5	299.2	20.7	43.1	106.1	63.0	20.8	156.2	109.5	27.3	11.8	197.6	75.2	595.1	45.3	14.9	27.7
CQ-7	mudstone	50.1	3.6	21.5	140.5	104.3	321.4	19.2	40.5	39.7	71.6	25.7	189.4	137.4	33.8	16.3	251.4	1.0	733.0	39.4	18.6	4.0
CQ-8	mudstone	48.6	3.5	18.3	108.4	110.0	307.5	18.9	41.7	41.5	73.3	24.5	189.4	136.4	27.6	15.4	208.2	3.4	708.3	38.6	17.9	3.7
CQ-9	mudstone	27.9	2.8	10.8	77.3	64.2	108.7	16.0	52.2	51.8	38.5	14.0	114.6	82.8	22.9	8.5	146.4	28.1	386.8	35.3	10.9	11.8
CQ-10	mudstone	48.7	3.4	19.4	125.3	97.3	317.6	18.9	40.5	37.1	71.0	24.5	184.3	140.5	31.2	15.3	230.1	1.1	705.4	38.2	17.2	3.7
CQ-11	mudstone	47.7	3.8	20.8	133.1	96.4	327.1	17.2	38.5	40.5	83.8	25.2	188.9	144.0	32.1	15.9	245.3	1.5	715.2	42.6	18.3	3.9
CQ-12	mudstone	45.7	3.5	19.9	129.0	91.9	371.5	18.6	37.7	34.9	71.8	23.8	183.2	140.1	28.9	14.9	243.0	1.0	701.4	37.7	16.2	3.6
CQ-13	mudstone	43.6	3.3	15.5	103.1	79.7	242.2	17.4	35.3	29.9	71.2	22.3	166.2	136.5	25.8	13.3	227.2	1.4	706.8	41.4	14.8	3.4
CQ-14	mudstone	40.4	3.2	24.8	133.6	88.8	4713.4	21.8	84.9	79.8	65.5	18.3	154.7	186.0	45.8	9.0	165.9	32.0	448.2	37.1	12.1	27.6
CQ-15	mudstone	35.0	2.2	13.2	90.1	94.2	2356.1	17.4	49.6	63.4	66.2	18.6	182.9	167.7	20.6	8.8	196.7	28.0	742.3	34.7	11.0	13.1
CQ-16	mudstone	17.7	1.6	8.7	90.9	42.0	3086.2	23.5	66.7	63.4	51.2	7.4	49.9	174.0	17.0	4.0	106.2	38.1	201.4	18.2	4.6	29.9
CQ-32	shale	35.1	2.9	14.5	91.5	125.5	251.6	20.3	49.0	79.8	69.8	21.0	148.1	152.9	23.6	15.0	266.0	1.3	689.8	33.0	16.6	3.6
CQ-33	shale	41.8	3.2	16.3	140.6	84.0	227.0	16.8	41.7	72.7	61.9	21.5	216.7	170.6	28.3	11.4	195.2	36.1	512.5	38.7	14.1	18.2
CQ-34	shale	33.7	6.0	12.9	101.3	106.2	884.3	17.1	65.7	61.3	54.4	19.7	256.2	127.3	26.1	19.6	175.1	25.9	437.6	52.6	15.0	11.9
CQ-35	shale	14.1	1.2	6.7	53.5	49.3	226.0	11.6	64.0	44.3	53.6	8.8	72.3	120.1	13.3	5.4	128.1	68.4	309.4	44.1	8.2	5.1
CQ-37	shale	27.8	1.5	6.3	256.9	37.5	120.9	12.7	34.6	140.5	33.0	12.7	61.0	76.7	13.0	5.4	63.2	131.0	729.5	35.6	7.6	73.3
CQ-38	shale	25.9	1.9	8.6	112.2	62.2	62.3	3.4	12.4	37.3	29.1	19.4	104.4	108.8	13.7	7.9	81.9	61.1	601.5	47.4	11.4	24.8
CQ-39	shale	25.7	2.3	9.6	186.5	48.7	124.6	14.2	32.4	130.6	45.1	16.2	79.5	106.3	21.4	7.9	102.3	75.0	467.6	35.1	9.2	45.1
CQ-40	shale	26.2	1.6	8.3	257.9	44.9	83.5	7.7	16.1	153.0	31.5	16.2	83.1	75.8	11.9	6.5	74.5	100.3	489.2	33.9	8.7	24.3
CQ-41	shale	20.9	1.9	5.0	108.9	45.5	89.3	11.6	23.6	98.2	35.8	17.1	61.8	74.3	8.2	6.8	81.1	76.4	285.0	41.1	4.1	24.1
CQ-42	shale	28.5	2.1	13.9	261.6	57.4	111.8	17.6	31.7	101.7	41.1	19.6	116.8	120.8	27.8	8.2	88.2	89.9	627.6	43.6	13.0	63.5
CQ-43	shale	13.0	1.7	6.2	120.4	31.1	98.0	5.9	14.5	78.8	27.1	16.9	93.2	107.9	21.6	8.7	177.9	98.4	673.2	44.8	13.0	34.6
CQ-44	shale	34.1	1.6	7.7	293.8	57.0	296.9	16.2	37.9	117.9	40.2	13.7	66.1	88.8	16.6	5.5	63.9	133.4	755.5	36.6	8.5	88.5
CQ-45	shale	20.7	2.5	14.9	203.1	70.7	328.7	16.8	53.6	134.1	56.7	15.8	93.3	110.5	37.0	6.5	151.2	116.4	459.5	30.0	7.9	74.8

Sample No	Lithology	Enrichment factor				Parameters						
		Mn_{EF}	Cu_{EF}	Mo_{EF}	U_{EF}	Sr/Ba	Sr/Cu	Ga/Rb	V/Cr	Zr/Rb	U/Th	δU
CQ-5	mudstone	0.33	1.16	0.65	1.32	0.22	2.77	0.16	1.28	2.14	0.24	0.84
CQ-6	mudstone	0.35	2.36	28.92	7.49	0.18	1.03	0.13	2.45	1.26	1.86	1.70
CQ-7	mudstone	0.38	0.88	0.38	1.08	0.19	3.46	0.14	1.35	1.33	0.22	0.79
CQ-8	mudstone	0.36	0.92	1.31	1.00	0.19	3.29	0.13	0.99	1.10	0.21	0.77
CQ-9	mudstone	0.13	1.15	10.81	3.19	0.21	1.60	0.12	1.20	1.28	1.09	1.53
CQ-10	mudstone	0.37	0.82	0.42	1.00	0.20	3.79	0.13	1.29	1.25	0.21	0.78
CQ-11	mudstone	0.38	0.90	0.58	1.05	0.20	3.56	0.13	1.38	1.30	0.21	0.78
CQ-12	mudstone	0.44	0.78	0.38	0.97	0.20	4.01	0.13	1.40	1.33	0.22	0.80
CQ-13	mudstone	0.28	0.66	0.54	0.92	0.19	4.57	0.13	1.29	1.37	0.23	0.81
CQ-14	mudstone	5.55	1.77	12.31	7.46	0.41	2.33	0.12	1.50	1.07	2.28	1.75
CQ-15	mudstone	2.77	1.41	10.77	3.54	0.23	2.65	0.10	0.96	1.08	1.20	1.56
CQ-16	mudstone	3.63	1.41	14.65	8.08	0.86	2.75	0.15	2.17	2.13	6.54	1.90
CQ-32	shale	0.30	1.77	0.50	0.97	0.22	1.92	0.14	0.73	1.80	0.34	0.79
CQ-33	shale	0.27	1.62	13.88	4.92	0.33	2.35	0.10	1.67	0.90	1.30	1.59
CQ-34	shale	1.04	1.36	9.96	3.22	0.29	2.08	0.08	0.95	0.68	0.80	1.41
CQ-35	shale	0.27	0.98	26.31	1.38	0.39	2.71	0.12	1.09	1.77	0.62	1.30
CQ-37	shale	0.14	3.12	50.38	19.81	0.11	0.55	0.21	6.85	1.03	9.66	1.93
CQ-38	shale	0.07	0.83	23.50	6.70	0.18	2.91	0.19	1.80	0.78	2.18	1.74
CQ-39	shale	0.15	2.90	28.85	12.19	0.23	0.81	0.20	3.83	1.29	4.91	1.87
CQ-40	shale	0.10	3.40	38.58	6.57	0.15	0.50	0.19	5.74	0.90	2.80	1.79
CQ-41	shale	0.11	2.18	29.38	6.51	0.26	0.76	0.28	2.40	1.31	5.88	1.89
CQ-42	shale	0.13	2.26	34.58	17.16	0.19	1.19	0.17	4.56	0.76	4.89	1.87
CQ-43	shale	0.12	1.75	37.85	9.35	0.16	1.37	0.18	3.87	1.91	2.66	1.78
CQ-44	shale	0.35	2.62	51.31	23.92	0.12	0.75	0.21	5.15	0.97	10.43	1.94
CQ-45	shale	0.39	2.98	44.77	20.22	0.24	0.82	0.17	2.87	1.62	9.44	1.93

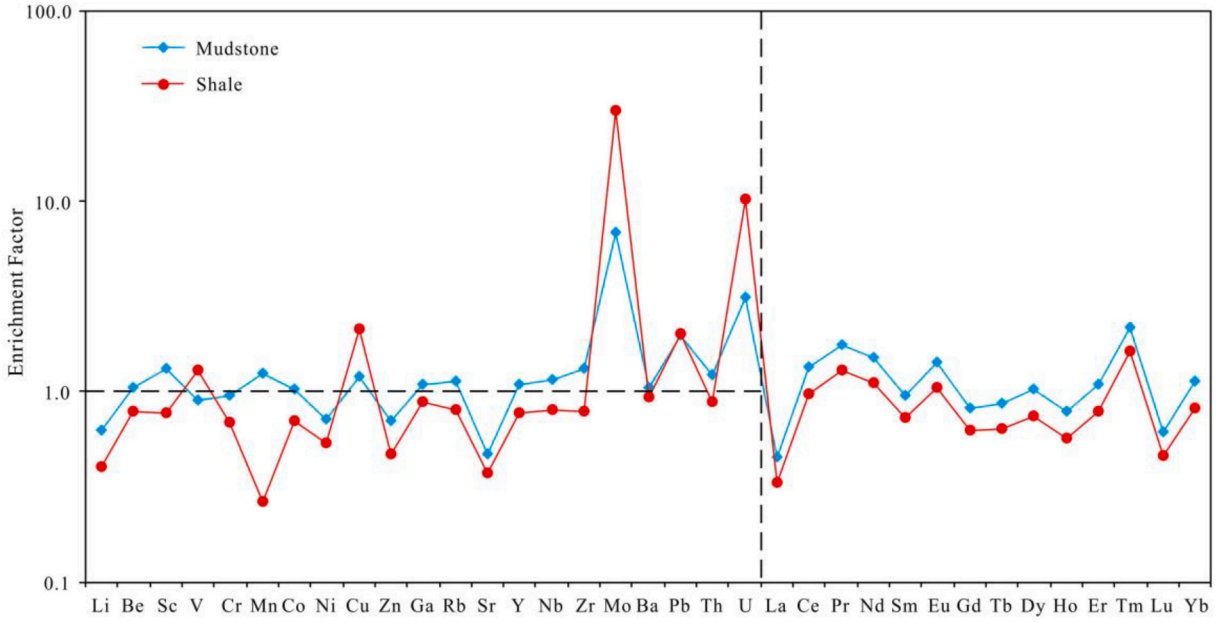

Fig. 3. The average enrichment factors of race elements and rare earth elements in the Chang 7 Member mudstone and shale, Ordos Basin (the element is considered enriched in the sample relative to the average content of shale composition in the Earth's crust; Turekian and Wedepohl, 1961).

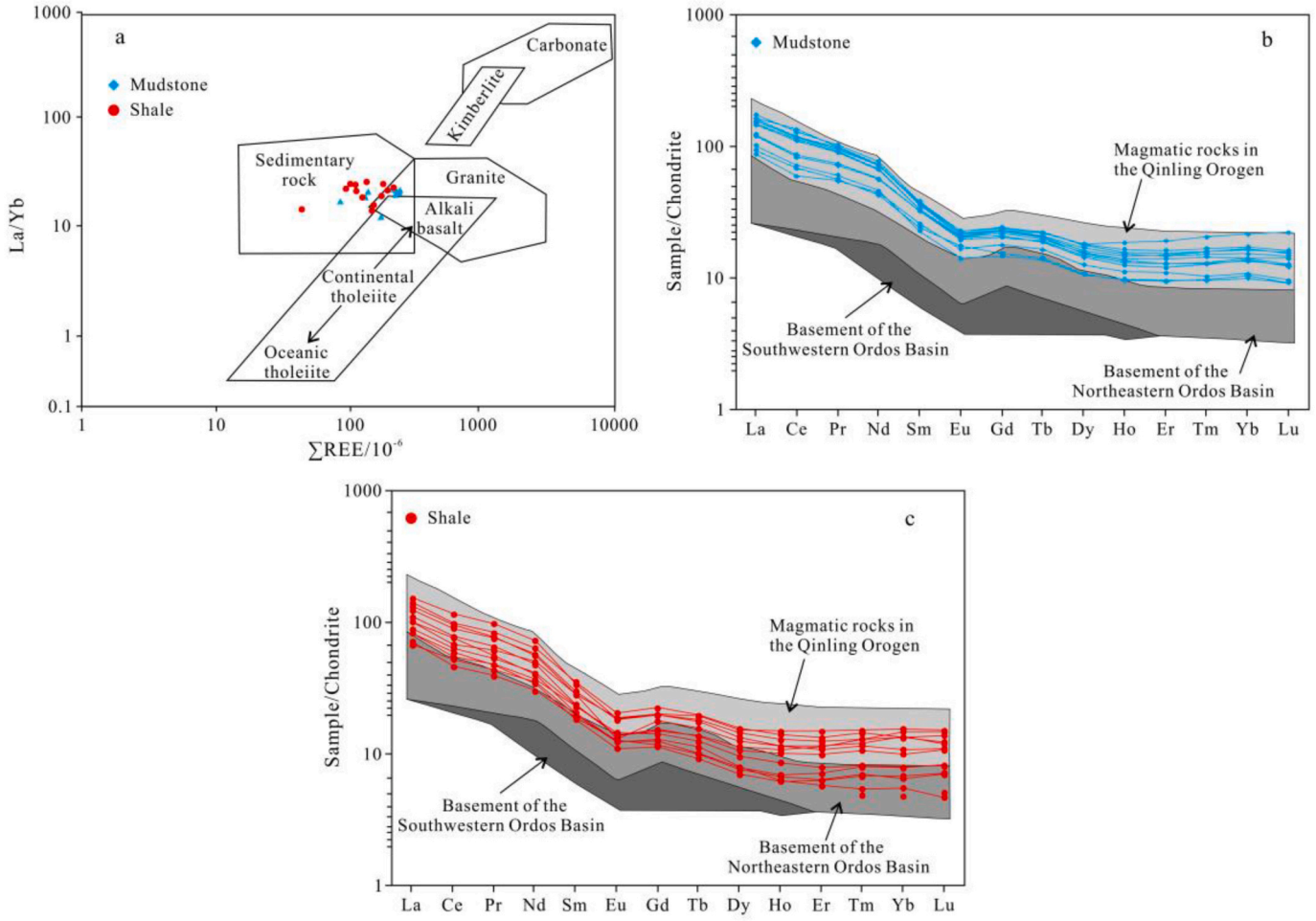

Fig. 4. Discrimination diagrams illustrating the provenance of the Chang 7 Member mudstones and shales (a. La/Yb vs. ∑REE diagram was proposed by Allègre and Minster (1978); b and c. REE chondrite-normalized distribution patterns, the date of magmatic rocks and basement rocks from Wang et al. (2013) and Luo et al. (2007)).

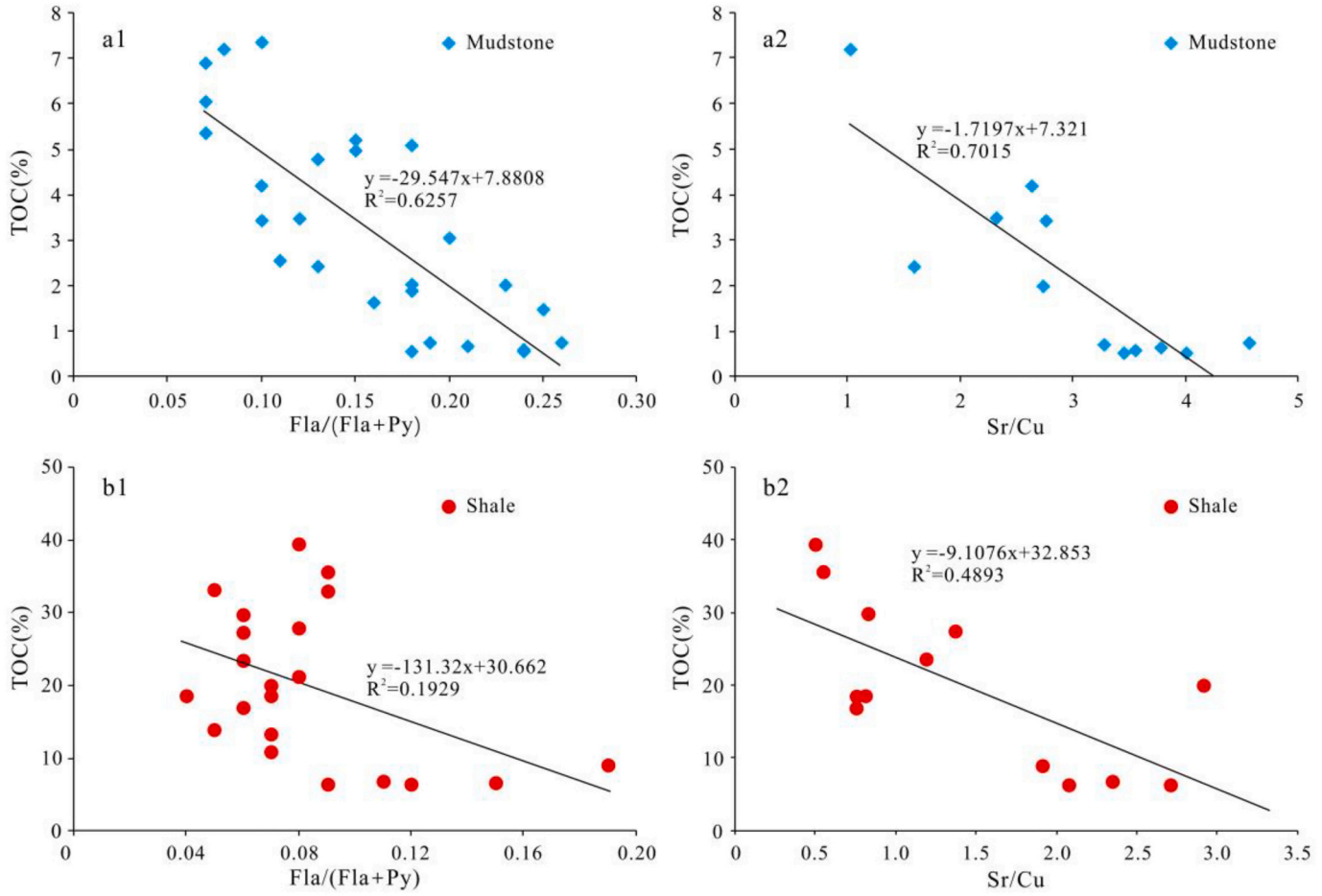

Fig. 5. The correlation between palaeoclimate and TOC in the Chang 7 Member shale and mudstone samples, Ordos Basin (a1 and b1: Fla./(Fal + Py) vs. TOC; a2 and b2: Sr/Cu vs. TOC).

(Table 3), and the values in the shale range from 0.50 to 51.31 and from 0.97 to 23.92, respectively (Table 3). The pattern of U–Mo covariation suggests that the mudstone formed under suboxic to anoxic conditions and the shale formed under anoxic to euxinic conditions (Fig. 9e). Moreover, the δU values (δU = 2 U/(U + Th/3)) > 1.0 and δU < 1.0 correspond to anoxic and aerobic environments, respectively (Steiner et al., 2001). The δU values of the Chang 7 Member shale and mudstone range from 0.79 to 1.94 (average 1.68) and from 0.77 to 1.90 (average 1.17), respectively (Table 3), suggesting that the shale was mainly deposited under a reducing environment and the mudstone was deposited under a weakly reducing environment.

As shown in Fig. 10, the Pr/Ph vs. TOC and δU vs. TOC in the mudstone show weakly positive correlations with R^2 values of 0.0483 and 0.4664, respectively (Fig. 10a1 and 10a2). The Pr/Ph vs. TOC in the shale shows a negative correlation with R^2 of 0.6330 (Fig. 10b1), whilst the δU vs. TOC in the shale shows a positive correlation with R^2 of 0.4082 (Fig. 10b2). As mentioned previously, lower Pr/Ph ratios correspond to a strong reducing environment and higher δU values indicate a higher reducing degree of the water column. Therefore, the redox conditions have a strong impact on organic-matter enrichment during the shale deposition, but have a weak impact on organic-matter enrichment during the mudstone deposition.

Accordingly, the shale deposition mainly occurred in anoxic conditions, whilst the mudstone deposition occurred in weakly suboxic conditions. An anoxic environment is conducive to organic-matter preservation, whilst an oxygenic environment causes the oxidation and degradation of organic matter. Therefore, an anoxic sedimentary environment is an important factor for preserving a large quantity of organic matter in shale, which is consistent with the research results of organic-matter enrichment of shale in other sedimentary basins (Cao et al., 2020; Zhang et al., 2021a; Khaled et al., 2022).

5.1.3.2. Palaeosalinity. Generally, the water stratification often occurs in the salt water column and forms an anoxic layer, which contributes to the preservation of organic matter. The gammacerane index (G/C_{30}H) is defined as the ratio of gammacerane to C_{30}-hopane, and it increases with the higher palaeosalinity of depositional environments (Moldowan et al., 1985). The G/C_{30}H values of the Chang 7 Member shale and mudstone vary from 0.02 to 0.11 (average: 0.06) and 0.09 to 0.24 (average: 0.14), respectively (Table 1). The results show that the shale was mainly deposited in a fresh-water environment and the mudstone was deposited mainly in a brackish-water environment. Moreover, the abundance of C_{26}-20S-TAS is high in the brackish and saline water, whilst the concentration of C_{28}-20S-TAS is high in the fresh water, and the saline water environment is characterised by C_{26}/C_{28}-20S-TAS > 0.45 (Meng et al., 2011; Xu et al., 2022). Therefore, the ratio of C_{26}/C_{28}-20S-TAS can be used to identify the salinity of sedimentary water; ratios of 0.20–0.45 and 0.45–0.94 correspond to the fresh water and brackish water, respectively (Xu et al., 2022). The C_{26}/C_{28}-20S-TAS ratios of the Chang 7 Member shale and mudstone range from 0.28 to 0.52 (average = 0.36) and from 0.24 to 0.62 (average = 0.38), respectively (Table 1), indicating that the shale and mudstone were mainly deposited in a fresh-water body, and the salinity of the water column during mudstone deposition is higher than that during shale deposition.

In addition, Sr and Ba are empirical indicators of palaeosalinity (Makeen et al., 2015; Wei and Algeo, 2020). Generally, a low Sr/Ba ratio

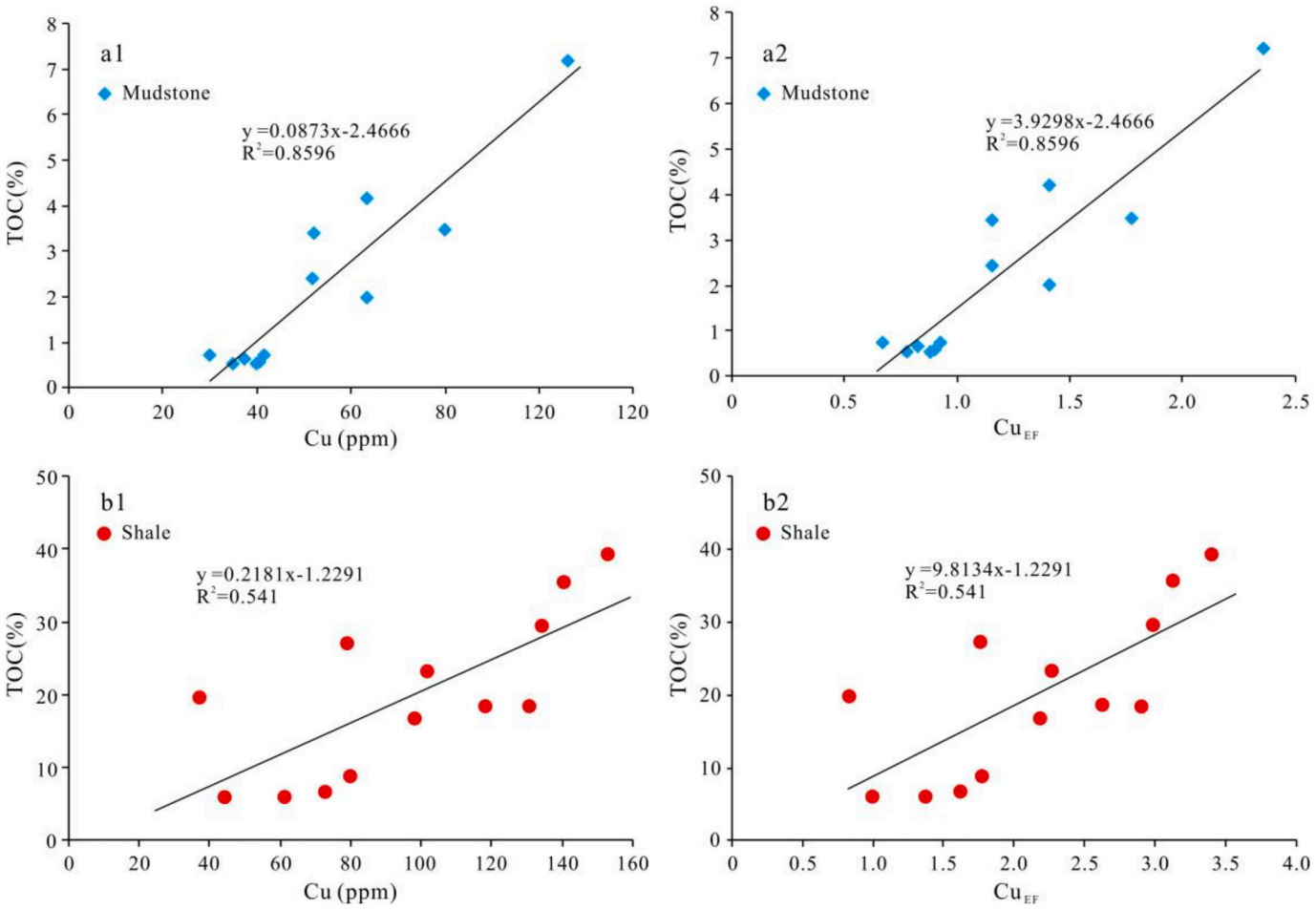

Fig. 6. The correlation between palaeoproductivity and TOC in the Chang 7 Member shale and mudstone samples, Ordos Basin (a1 and b1: Cu vs. TOC; a2 and b2: Cu_{EF} vs. TOC).

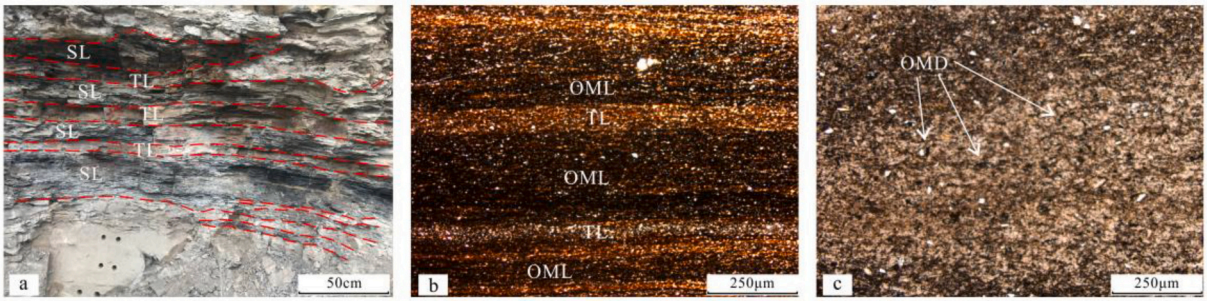

Fig. 7. Field outcrop and core photomicrographs of the Chang 7 shale and mudstone. (a) Interbedded distribution of tuff and shale in the YSC outcrop; (b) Lamellar structure of organic-matter and volcanic ash laminae, thin section (reflected light), well C75 (CQ-32); (c) Debris structure of organic-matter, thin section (reflected light), well C75 (CQ-6). Note: SL = shale layer, TL = tuff layer, OML = organic matter layer, OMD = organic matter debris.

(< 0.2) indicates fresh water, a moderate ratio (0.2–0.5) indicates brackish water and a high one (> 0.5) indicates saline water (Wei and Algeo, 2020). The Sr/Ba ratios of the Chang 7 Member shale and mudstone range from 0.11 to 0.39 (average = 0.22) and from 0.18 to 0.86 (average = 0.27), respectively (Table 3), indicating that the shale was deposited in fresh to brackish water, and the mudstone was deposited in a fresh to saline water.

As shown in Fig. 11, there is no obvious correlation between $G/C_{30}H$, C_{26}/C_{28}-20S-TAS, Sr/Ba and TOC in the Chang 7 Member mudstone with R^2 values of 0.0459, 0.0358 and 0.0015 (Fig. 11a1–a3). The $G/C_{30}H$, C_{26}/C_{28}-20S-TAS, Sr/Ba and TOC correlations show negative correlations with R^2 values of 0.5503, 0.5286 and 0.5395 in the Chang 7 Member shale (Fig. 11b1–b3). Thus, these results indicate that the palaeosalinity conditions have a negative impact on the organic-matter enrichment during the shale deposition, whilst it has no obvious impact on the organic-matter enrichment during the mudstone deposition.

There is an organic compound called dimethylsulphoniopropionate (DMSP) in marine phytoplankton, algae and vascular plants, and they can adapt to the changes of external salinity by adjusting their DMSP concentration (Wolfe et al., 1997). The organic matter of the Chang 7 Member shale is mainly composed of fresh-water algae (such as cyanobacteria, green algae and golden algae) (Zhang et al., 2016). Due to

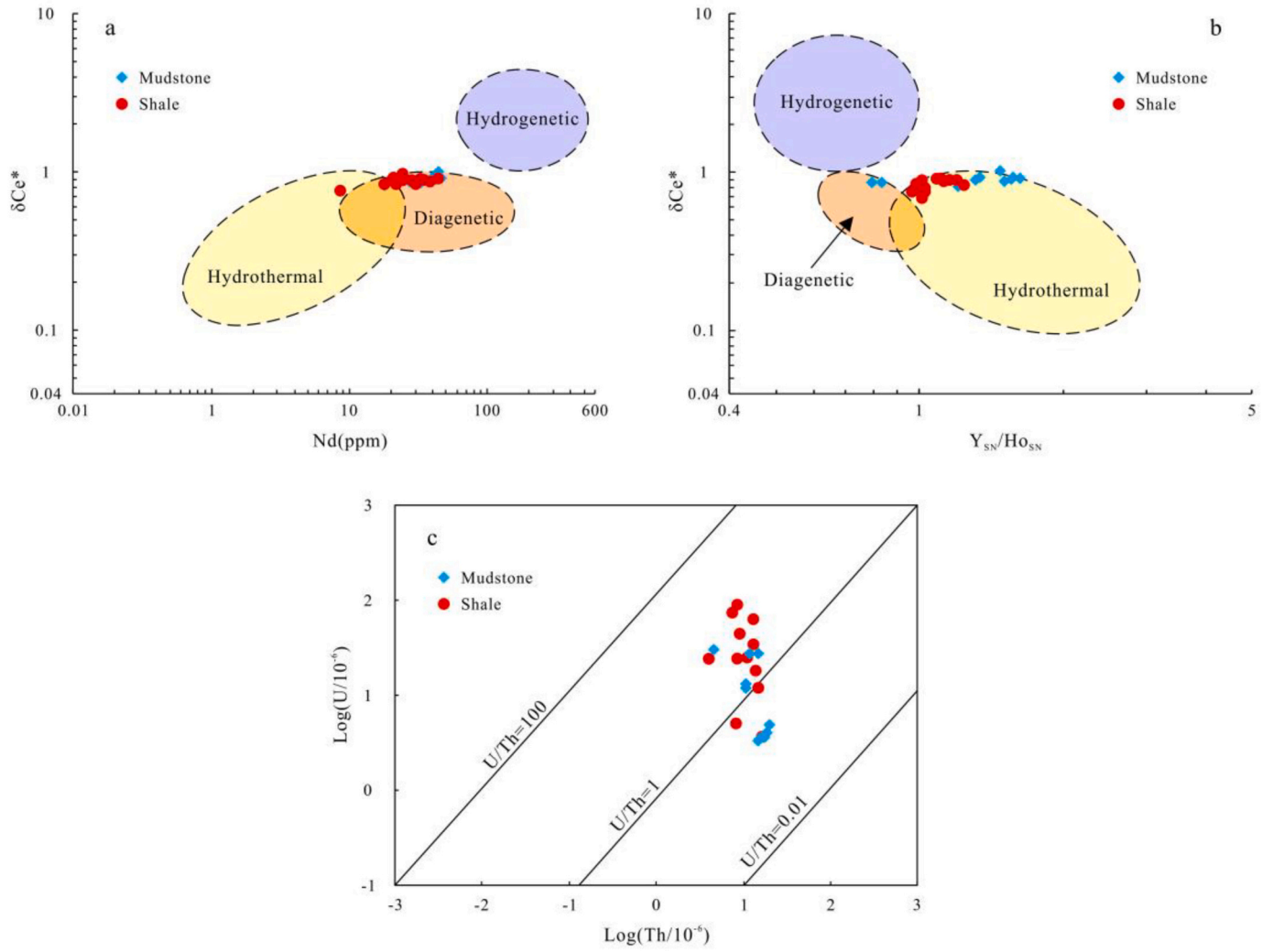

Fig. 8. Hydrothermal activity discriminant plots of a. Nd vs. δCe* (after Bua et al., 2014), b. Y_{SN}/Ho_{SN} vs. δCe* (after Bua et al., 2014), c. Lg ($Th/10^{-6}$) vs. Lg ($U/10^{-6}$) (after Bostrom, 1983). Note: $\delta Ce^* = 2Ce_{SN}/(La_{SN} + Pr_{SN})$. The subscript SN represents the shale of PAAS; Mclennan, 1989.

the lack of the DMSP, these fresh-water algae are very sensitive to salinity changes in the sedimentary environment, and their growth ability will decrease with increased salinity (Liu et al., 2022). The mudstone was deposited in a brackish-water environment, and its organic matter is a mixture of fresh-water algae and higher plants. Therefore, the influence of salinity on the organic-matter enrichment of shale is higher than that of mudstone.

5.1.3.3. Water depth. In general, affected by the growth of aquatic plants and the distribution of aerobic organisms, the strength of illumination decreases with increased water depth (Rao and Huang, 2017). Therefore, deep-water areas are more likely to form an anoxic sedimentary environment, which is more conducive to organic-matter preservation. Zr and Rb are concentrated in coarse and fine particles, respectively. Generally speaking, the average size of sediments decreases with increased water depth. Therefore, the Zr/Rb ratio can be used to indicate the variation of palaeowater depth (Dypvik and Harris, 2001). Higher ratios correspond to shallow water and lower ratios correspond to deep-water environments.

In our study, the Zr/Rb ratios of the Change 7 Member shale and mudstone samples range from 0.68 to 1.91 (average = 1.20) and from 1.07 to 2.14 (average = 1.39), respectively (Table 3). The relatively low Zr/Rb ratios in the shale samples indicate that the water depth during their deposition was greater than that during mudstone deposition. Therefore, compared with shale, the organic-matter composition of mudstone is more easily affected by the input of terrestrial organic matter, which is consistent with the greater content of terrestrial organisms in the mudstone organic matter than in shale organic matter.

As shown in Fig. 12, there is no obvious correlation between Zr/Rb and TOC in mudstone and shale of the Chang 7 Member, with R^2 values of 0.0002 and 0.0054, respectively, indicating that palaeowater depth is not the main factor affecting the organic-matter enrichment during mudstone and shale deposition.

5.1.4. Dilution effect

Dilution is defined as the sedimentation rate of terrestrial detrital matter in lacustrine and marine depositional environments. The sedimentation rate plays an important role in organic-matter enrichment. A sedimentation rate that is too high causes organic matter to be diluted by siliceous debris, whilst a sedimentation rate that is too slow causes organic matter to be oxidised and biodegraded during preservation (Johnson Ibach, 1982; Tyson, 2001; Ding et al., 2015).

The LREEs are generally adsorbed by organic matter and clay minerals, whilst the HREEs form stable complexes in lake water (Chen et al., 2019). Thus, the differentiation degree of REEs can reflect sedimentation-rate changes. High LREE/HREE ratios and $(La/Yb)_N$ values (the subscript N represents the North American Shale Composite; Gromet et al., 1984) correspond to low sedimentation rates, whilst low

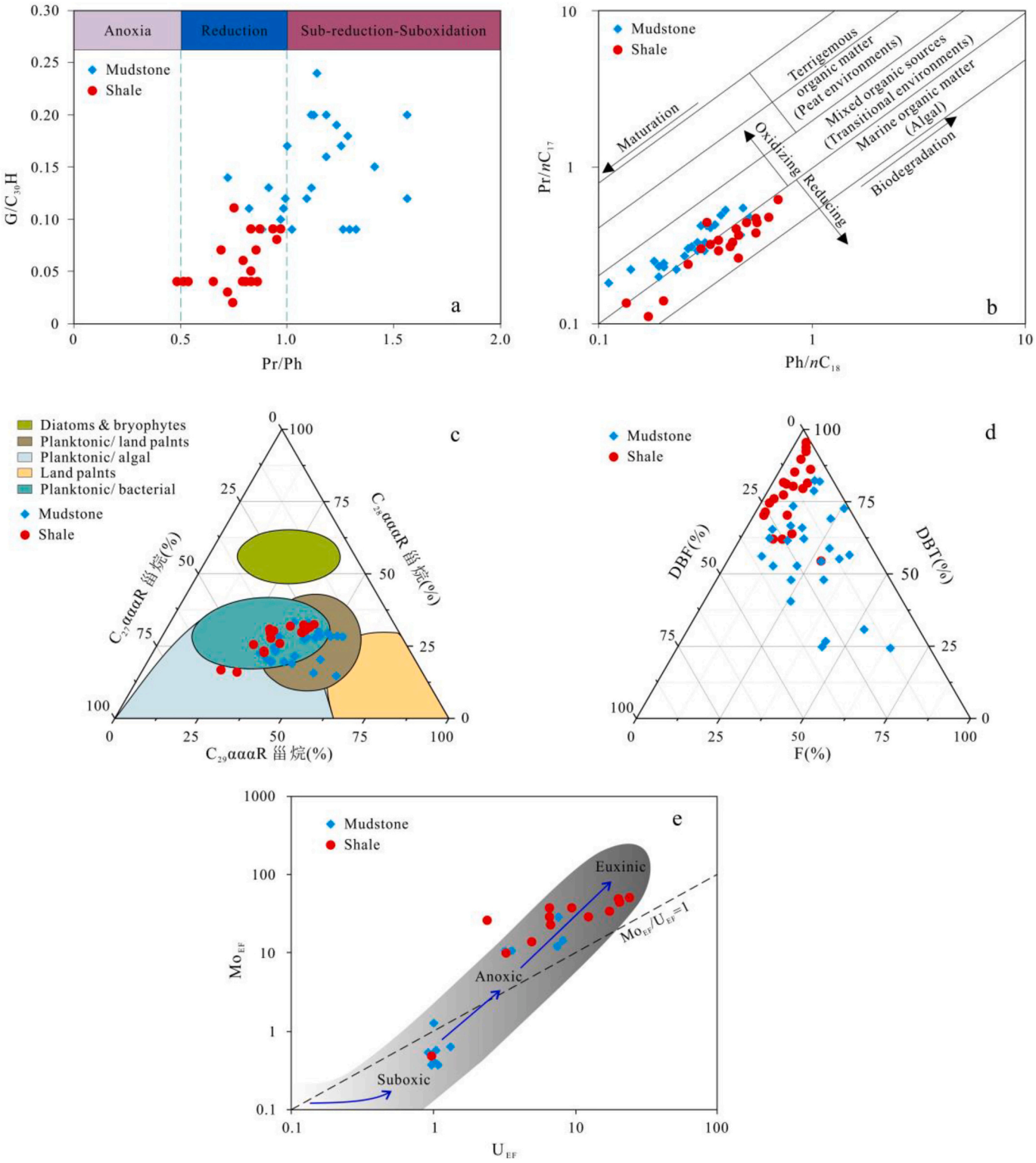

Fig. 9. Cross plots of Pr/Ph vs. $G/C_{30}H$ (a), Pr/nC_{17} vs. Ph/nC_{18} (b), C_{27}-C_{28} - C_{29} ααα*R* steranes ternary(c), DBT-BDF- F ternary (d) and the cross plots of Mo_{EF} vs. U_{EF} (modified from Algeo and Tribovillard, 2009) showing the palaeoenvironment for the Chang 7 Member shale and mudstone, Ordos Basin.

values correspond to high sedimentation rates (Elderfield and Greaves, 1982; Goldstein and Jaconbsen, 1988). The LREE/HREE ratios of the Chang 7 Member mudstone and shale samples vary from 6.47 to 10.96 (average = 9.41) and from 6.75 to 12.32 (average = 9.51), respectively (Table 2). The $(La/Yb)_N$ values of the Chang 7 Member mudstone and shale samples vary from 0.79 to 1.62 (average = 1.36) and from 0.95 to 1.87 (average = 1.47), respectively (Table 2). The mineralogical composition of the Chang 7 Member mudstone and shale is clay minerals and quartz. Mudstone is characterised by relatively less clay mineral content (43.4%) and more quartz (21.5%), and the shale has the characteristics of relatively more clay mineral content (52.1%) and less quartz (12.5%) (Lin et al., 2017; Liu et al., 2018). The high LREE/HREE ratios and $(La/Yb)_N$ values of shale are consistent with its high clay mineral content. These results suggest that the sedimentation rate of

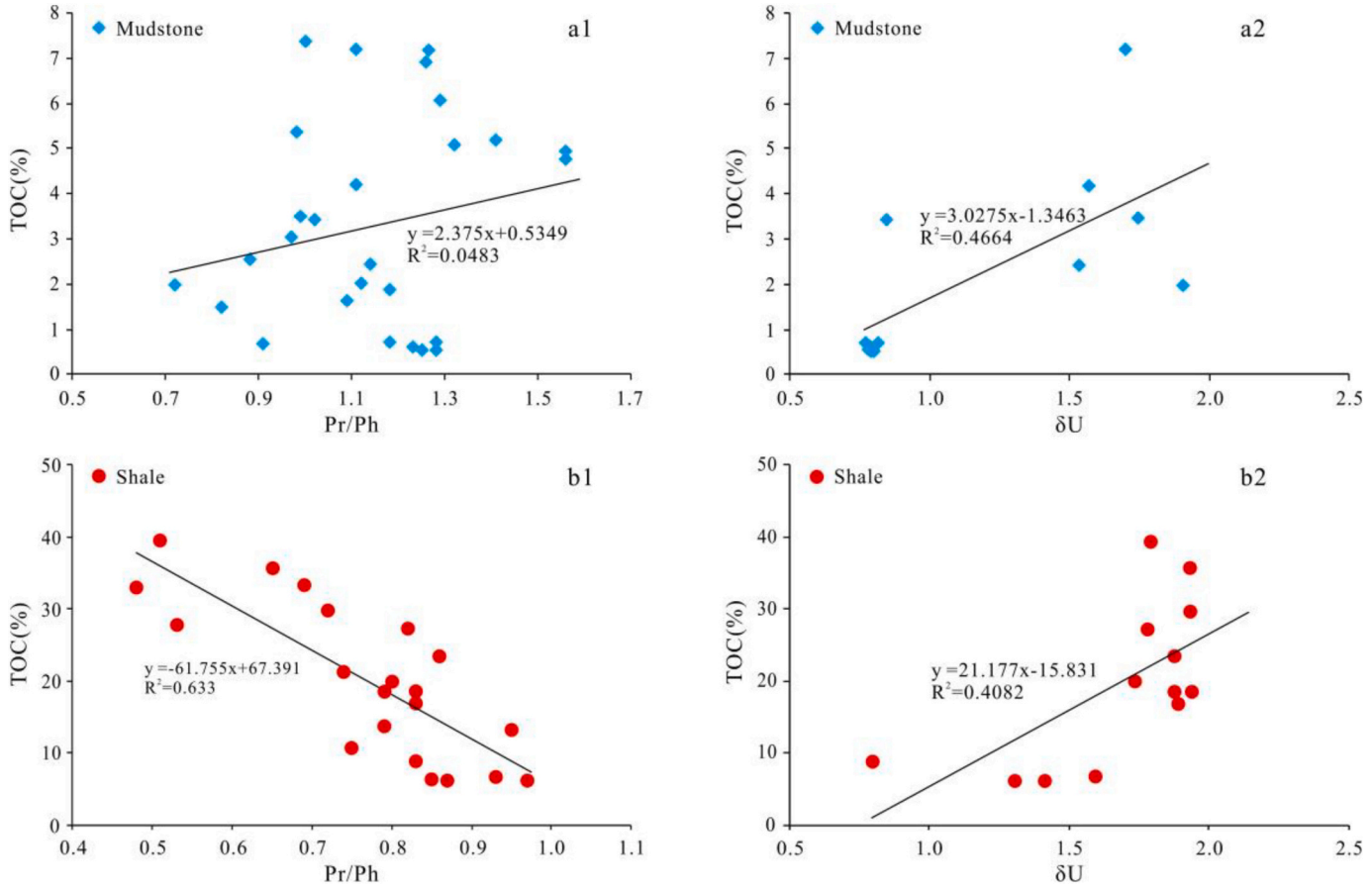

Fig. 10. The correlation between redox conditions and TOC in the Chang 7 Member shale and mudstone samples, Ordos Basin (a1 and b1: Pr/Ph vs. TOC; a2 and b2: δU vs. TOC).

shales was lower than that of mudstones in the Chang 7 Member.

As shown in Fig. 13, the LREE/HREE vs. TOC and $(La/Yb)_N$ vs. TOC plots show negative correlations, with R^2 values of 0.3773 and 0.6024 in the Chang 7 Member mudstone, respectively (Fig. 13a1 and 13a2). There is no obvious correlation between LREE/HREE ratio or $(La/Yb)_N$ value and TOC in the Chang 7 Member shale with R^2 values of 0.0001 and 0.0317 (Fig. 13b1 and b2). The results indicate that the sedimentation rate had an obvious effect on the organic-matter enrichment during the mudstone deposition, and it had no obvious impact on the organic-matter enrichment during the shale deposition.

Consequently, affected by the warmer and wetter palaeoclimate, the massive input of terrigenous clastic rocks made the sedimentation rate of mudstone higher than that of shale. The high sedimentation rate caused the dilution of organic matter in mudstone, resulting in the decreased abundance of organic matter in the mudstone. Therefore, the hydrocarbon generation potential of shale is higher than that of mudstone.

5.2. *Enrichment mechanism of organic matter*

5.2.1. *Chang 7 Member shale*

During the shale deposition (Chang 7^3), tectonic activities resulted in the formation of a deep lacustrine sub-facies (Yang et al., 2010). During this period, the palaeoclimate was drier than that during mudstone deposition, which was not conducive to the large-scale growth of terrestrial higher plants (conifers). Thus, there are few terrestrial organisms in the shale organic matter. However, influenced by the nutrient elements (Cu, Mo and Pb) carried by the parent rocks, volcanic ash and hydrothermal fluid, phytoplankton and algae grew on a large scale. As a result, the palaeoproductivity of the water column was greatly improved. Concurrently, the bloom of bacteria consumed oxygen and formed an anoxic preservation condition. Anoxic water column avoided the oxidisation and biodegradation of organic matter, and low sedimentation rate also avoided the dilution of organic matter by siliceous elastics. Therefore, the nutrients carried by the parent rocks and geological events increased the lake basin primary productivity during the shale deposition. The anoxic sedimentary environment and low sedimentation rate preserved the organic matter, so the shale has a high abundance of organic matter.

As discussed above, redox conditions, palaeoproductivity and palaeosalinity are significantly correlated with the organic-matter abundance of shale, whilst palaeoclimate, palaeowater depth and sedimentation rate are weakly correlated with the abundance. Palaeosalinity impacted the palaeoproductivity by affecting the growth of phytoplankton and algae, in turn affecting the organic-matter enrichment of shale. Therefore, high palaeoproductivity and anoxic preservation conditions are the predominant influencing factors of the organic-matter enrichment in the Chang 7 Member shale. The organic-matter enrichment in the Chang 7 Member shale follows a high palaeoproductivity and anoxic preservation model (Fig. 14a).

5.2.2. *Chang 7 Member mudstone*

During the mudstone deposition (Chang 7^1 and Chang 7^2), tectonic activities resulted in shallow lacustrine to semi-deep lacustrine sub-facies (Yang et al., 2010). During this period, the palaeoclimate was very warm–humid, which contributed to the large-scale growth of terrestrial higher plants (such as conifers). Thus, the organic matter of mudstone contained a large quantity of terrestrial organisms. In addition, influenced by the nutrient elements (Mn, Cu, Mo and Pb) carried by the parent rocks and hydrothermal fluid, phytoplankton and algae were also relatively prosperous. But the suboxic water column caused the

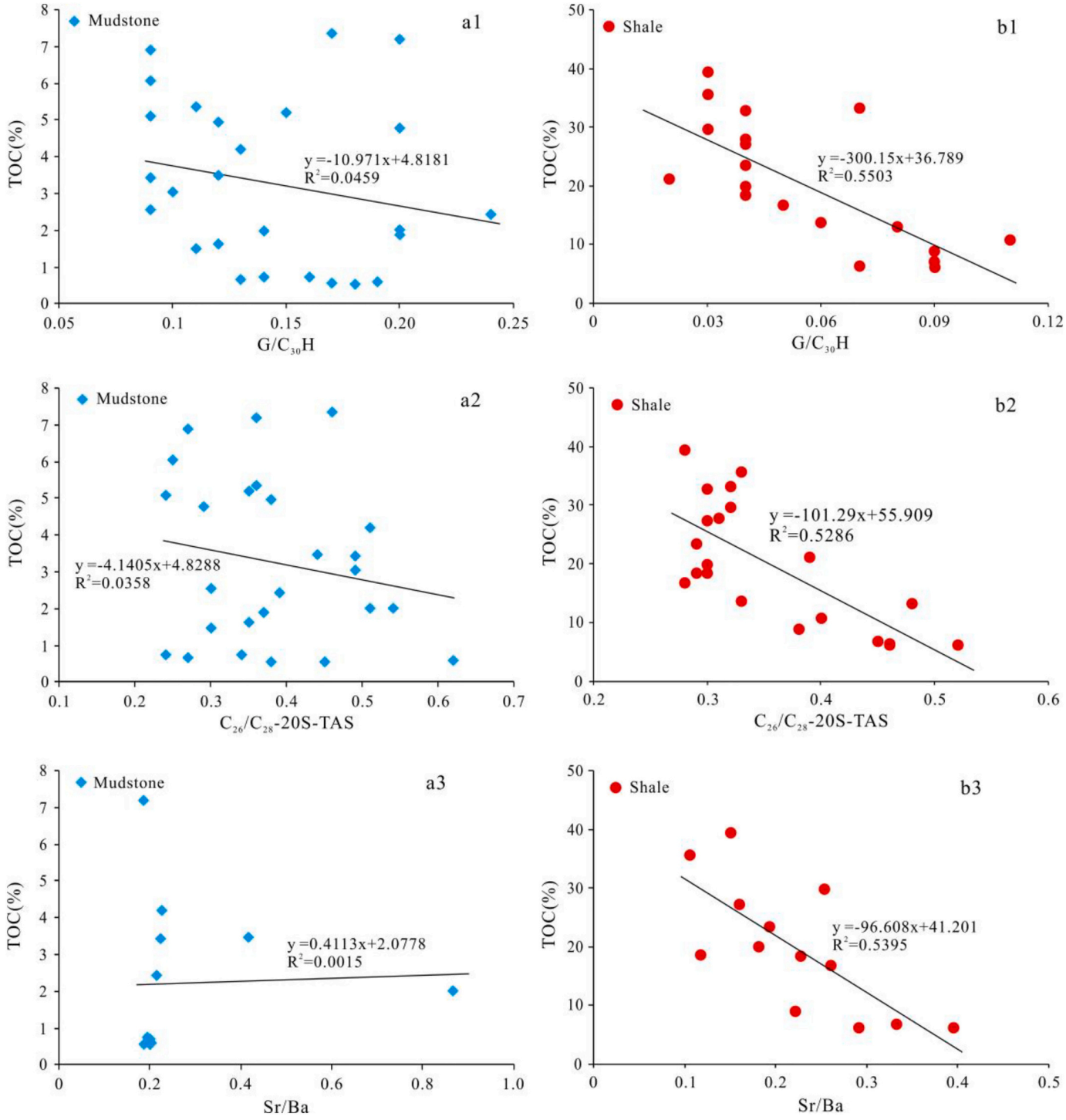

Fig. 11. The correlation between palaeosalinity and TOC in the Chang 7 Member shale and mudstone samples, Ordos Basin (a1 and b1: $G/C_{30}H$ vs. TOC; a2 and b2: C_{26}/C_{28}-20S-TAS vs. TOC; a3 and b3: Sr/Ba vs. TOC).

oxidation and degradation of organic matter in the process of mudstone deposition, and the high sedimentation rate diluted the organic matter in the mudstone sediments. Therefore, the input of a large quantity of terrestrial nutrients provided only moderate primary productivity during the deposition of mudstone. The oxygenic sedimentary environment and high sedimentation rate did not well preserve the organic matter; therefore, the mudstone has low organic-matter abundance.

As discussed previously, palaeoclimate, palaeoproductivity and sedimentation rate are significantly correlated with the organic-matter abundance of mudstone, whilst reducing conditions, palaeosalinity and palaeowater depth are weakly correlated with the abundance. Palaeoclimate affected the palaeoproductivity by affecting the growth of terrestrial higher plants, in turn affecting the organic-matter enrichment of mudstone. Therefore, moderate palaeoproductivity and high sedimentation rate are the predominant influencing factors of the organic-matter enrichment in the Chang 7 Member mudstone. The organic-matter enrichment in the Chang 7 Member mudstone follows a moderate palaeoproductivity and high dilution model (Fig. 14b).

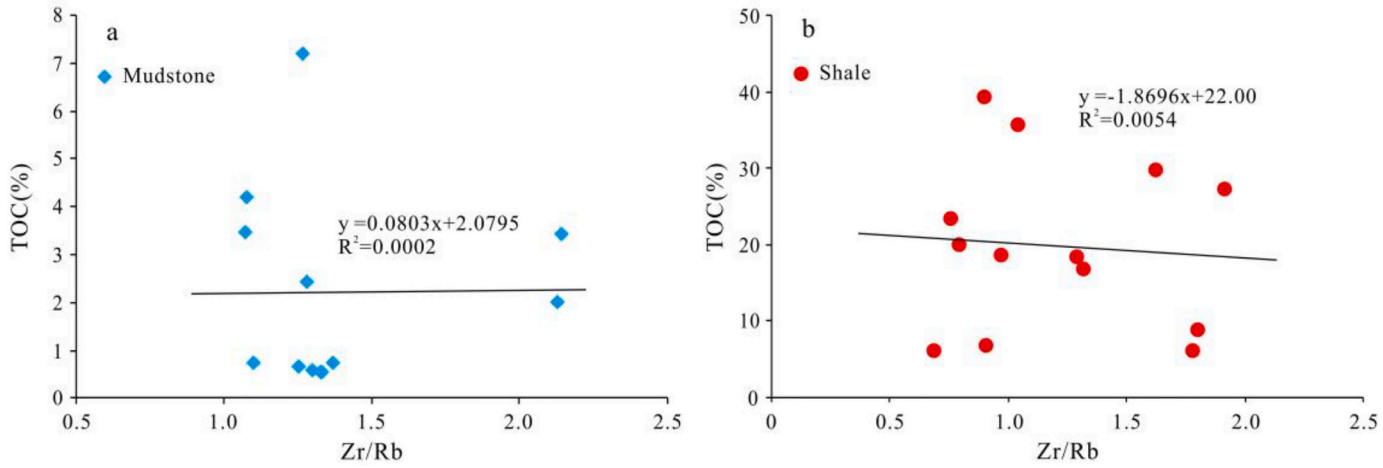

Fig. 12. The correlation between palaeowater depth and TOC in the Chang 7 Member shale and mudstone samples, Ordos Basin.

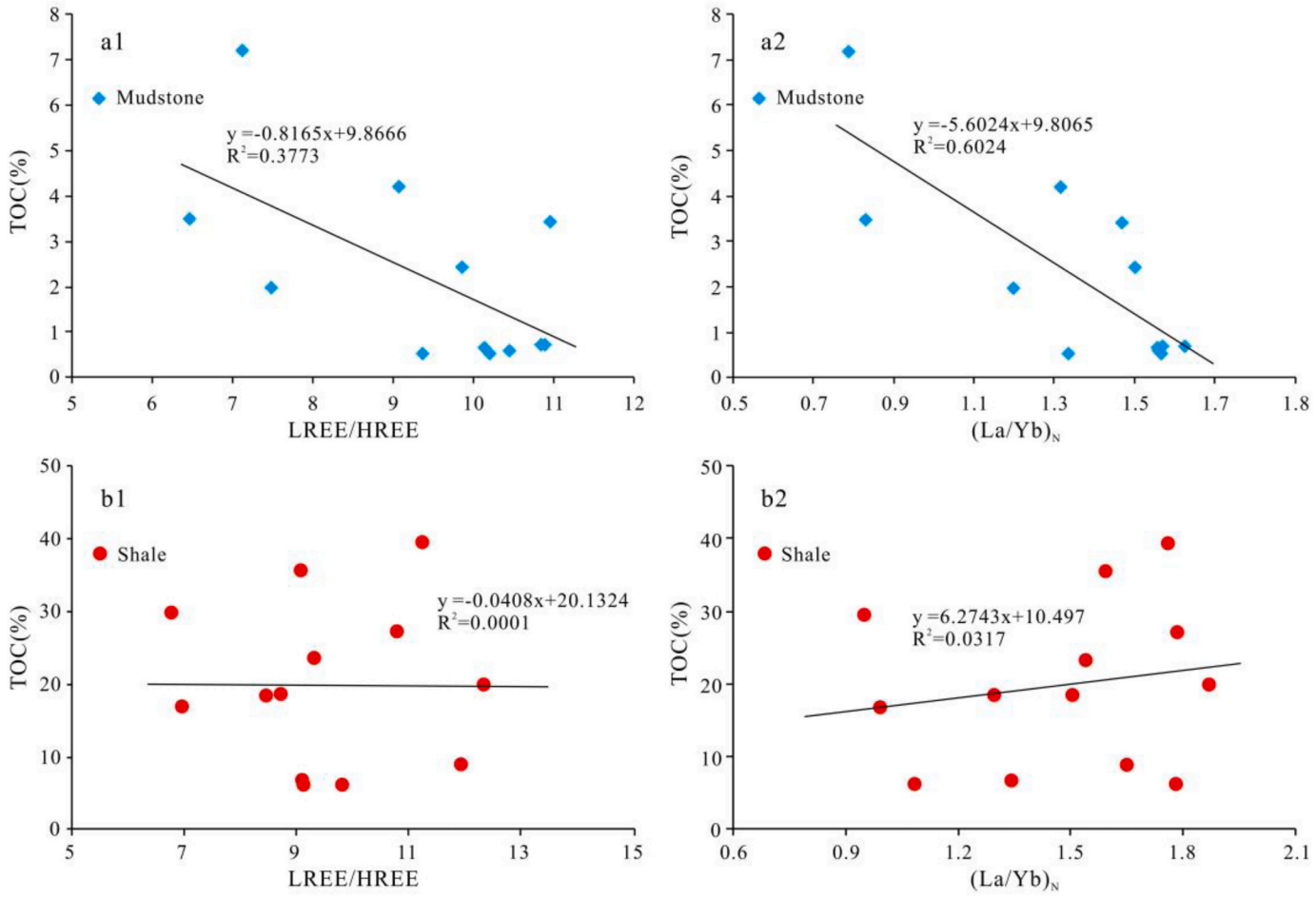

Fig. 13. The correlation between sedimentation rate and TOC in the Chang 7 Member shale and mudstone samples, Ordos Basin (a1 and b1: LREE/HREE vs. TOC; a2 and b2: $(La/Yb)_N$ vs. TOC). Note: The subscript N represents the North American Shale Composite; Gromet et al., 1984.

6. Conclusions

Cores and outcrop samples of the Chang 7 Member mudstone and shale in the Ordos Basin were analysed for biomarkers and element geochemical parameters. The main controlling factors and models of organic-matter enrichment in the Chang 7 Member mudstone and shale were as follows:

(1) The parent rocks of mudstone and shale in the Chang 7 Member are a mixture of sedimentary rock and granite, but the material source is different. The material source of mudstone was mainly from the southern Ordos Basin, whilst that of shale was mainly from the southern and northeastern Ordos Basin.

(2) The shale was mainly deposited under reducing conditions with organic matter that is mainly composed of algae, and the

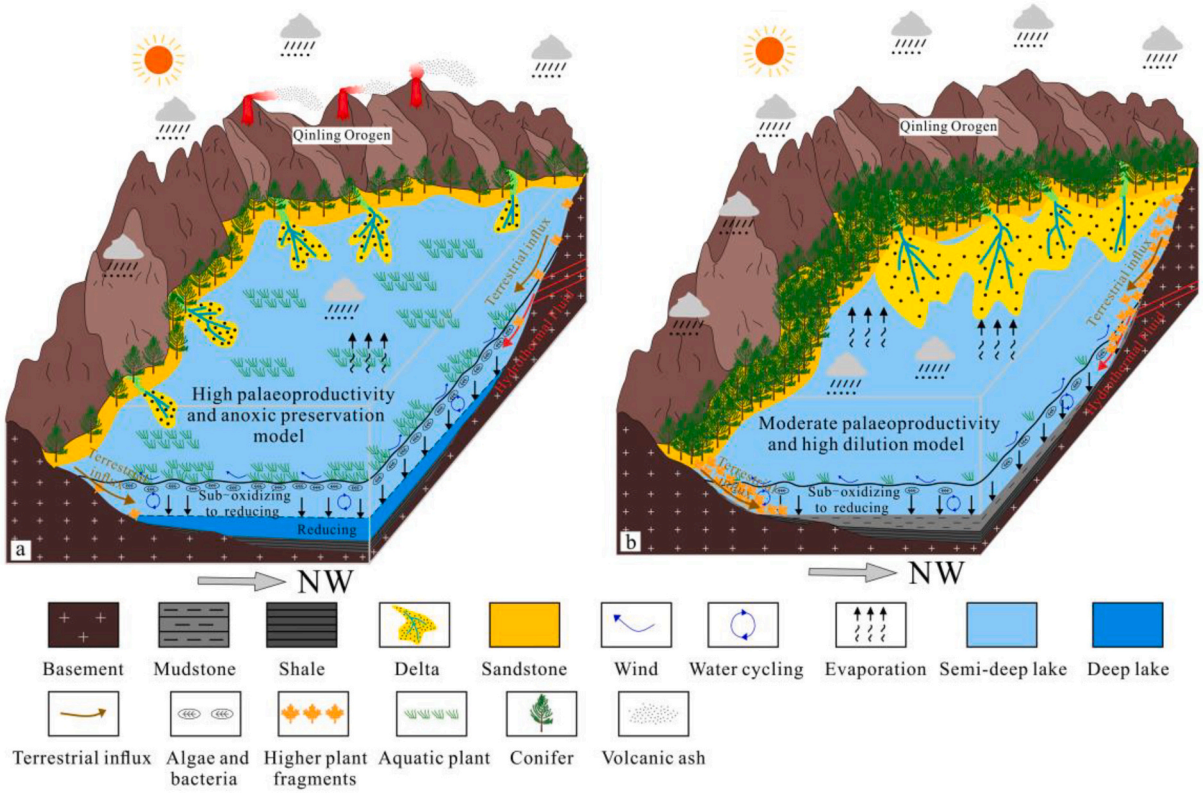

Fig. 14. The organic-matter enrichment models of the Chang 7 Member shale (a) and mudstone (b).

mudstone was mainly deposited under weakly oxidising to weakly reducing conditions with organic matter that is a mixture of algae and higher plants. The salinity of the water column and the sedimentation rate during mudstone deposition were higher than those during shale deposition, and the water depth during shale deposition was larger than that of mudstone.

(3) The nutrients carried by parent rocks, volcanic ash and hydrothermal fluid created large-scale phytoplankton and algae growth during the deposition of shale, so the lake basin had high palaeoproductivity. In addition, anoxic deposition conditions were conducive to the preservation of a large amount of organic matter in shale, resulting in high hydrocarbon generation potential of the Chang 7 Member shale.

(4) The warmer and wetter palaeoclimate made the terrestrial higher plants (conifers) growth increase on a large scale during the deposition of mudstone, and the input of a large quantity of terrestrial nutrients gave the lake basin moderate palaeoproductivity. However, due to the high sedimentation rate the organic matter was diluted, resulting in low hydrocarbon generation potential of the mudstone in the Chang 7 Member.

Declaration of Competing Interest

The authors declare that they have no known competing financial interests or personal relationships that could have appeared to influence the work reported in this paper.

Acknowledgements

The corresponding author of this study was financially supported by the China National Petroleum Corporation and China University of Petroleum (Beijing) for this Cooperation Science and Technology Project (Grant No. ZLZX2020-02-01-01). We sincerely thank two anonymous reviewers for their detailed and constructive comments that significantly improved the manuscript. We also sincerely thank Prof. Luofu Liu from China University of Petroleum–Beijing for polishing the language of the manuscript.

References

Afify, A.M., Sanz-Montero, M.E., Calvo, J.P., 2018. Differentiation of ironstone types by using rare earth elements and yttrium geochemistry–a case study from the Bahariya region, Egypt. Ore Geol. Rev. 96, 247–261.

Akinlua, A., Adekola, S.A., Swakamisa, O., Fadipe, O.A., Akinyemi, S.A., 2010. Trace element characterization of Cretaceous Orange Basin hydrocarbon source rocks. Appl. Geochem. 25, 1587–1595.

Algeo, T.J., Tribovillard, N., 2009. Environment analysis of paleoceanographic systems based on molybdenum – uranium covariation. Chem. Geol. 268, 211–225.

Allègre, C.J., Minster, J.F., 1978. Quantitative models of trace element behavior in magmatic processes. Earth Planet. Sci. Lett. 38 (1), 1–25.

Armstrong-Altrin, J.S., Machain- Castillo, M.L., Rosales-Hoz, L., Carranza-Edwards, A.C., Sanchez-Cabeza, J.A., RuÍz-Fernández, A.C., 2015. Provenance and depositional history of continental slope sediments in the Southwestern Gulf of Mexico unraveled by geochemical analysis. Cont. Shelf Res. 95, 15–26.

Arsairai, B., Wannakomol, A., Feng, Q.L., Chonglakmani, C.P., 2016. Paleoproductivity and paleoredox condition of the Huai Hin Lat Formation in Northeastern Thailand. J. Earth Sci. 27 (3), 350–364.

Arthur, M.A., Sageman, B.B., 1994. Marine black shales: depositional mechanisms and environments of ancient deposits. Annu. Rev. Earth Planet. Sci. 1994 (22), 499–551.

Bau, M., Schmidt, K., Koshinsky, A., Hein, J., Kuhn, K., Usui, A., 2014. Discriminating between different genetic types of marine ferro-manganese crusts and nodules based on rare earth elements and yttrium. Chem. Geol. 381, 1–9.

Bhatia, M.R., Taylor, S.R., 1981. Trace-element geochemistry and sedimentary provinces: a study from the Tasman Geosyncline, Australia. Chem. Geol. 33 (1–4), 115–125.

Bostrom, K., 1983. Genesis offeeromanganese deposits-diagnositic criteria for recent and old deposits. In: Hydrothermal Processes at Seafloor Spreading Centers. Springer, US, pp. 473–489.

Canfield, D.E., 1989. Reactive iron in marine sediments. Geochim. Cosmochim. Acta 53 (3), 619–632.

Canfield, D.E., 1994. Factors influencing organic carbon preservation in marine sediments. Chem. Geol. 114 (3–4), 315–329.

Cao, L., Zhang, Z.H., Li, H.Y., Zhong, N.N., Xiao, L.L., Jin, X., Li, H., 2020. Mechanism for the enrichment of organic matter in the Liushagang Formation of the Weixinan Sag, Beibuwan Basin, China. Mar. Pet. Geol. 122, 104649.

Chen, H., Tang, D.Z., Chen, S.D., Tang, S.L., 2022. Geochemical characteristics of mudstones from the lower cretaceous strata of the Jixi Basin, NE China: Implications for organic matter enrichment. Int. J. Coal Geol. 249, 103904.
Chen, Y.H., Zhu, Z.W., Zhang, L., 2019. Control actions of sedimentary environments and sedimentation rates on lacustrine oil shale distribution, an example of the oil shale in the Upper Triassic Yanchang Formation, southeastern Ordos Basin (NW China). Mar. Pet. Geol. 102, 508–520.
Chen, Z.H., Guo, Q.L., Jiang, C.Q., Liu, X.J., Reyes, J., Mort, A., Jia, Z.K., 2017. Source rock characteristics and Rock-Eval-based hydrocarbon generation kinetic models of the lacustrine Chang-7 Shale of Triassic Yanchang Formation, Ordos Basin, China. Int. J. Coal Geol. 182, 52–65.
Crombez, V., Baudin, F., Rohais, S., Riquier, L., Euzen, T., Pauthier, S., Ducros, M., Caron, B., Vaisblat, N., 2017. Basin scale distribution of organic matter in marine fine-grained sedimentary rocks: Insight from sequence stratigraphy and multi-proxies analysis in the Montney and Doig Formations. Mar. Pet. Geol. 83, 382–401.
Demaison, G.J., Moore, G.T., 1980. Anoxic environments and oil source bed genesis. Org. Geochem. 2 (1), 9–31.
Ding, X.J., Liu, G.D., Zha, M., Huang, Z.L., Gao, C.H., Lu, X.J., Sun, M.L., Chen, Z.L., LiuZhang, X.X., 2015. Relationship between total organic carbon content and sedimentation rate in ancient lacustrine sediments, a case study of Erlian basin, northern China. J. Geochem. Explor. 149, 22–29.
Dypvik, H., Harris, N.B., 2001. Geochemical facies analysis of fine-grained siliciclastics using Th/U, Zr/Rb and (Zr+Rb)/Sr ratios. Chem. Geol. 181, 131–146.
Elderfield, H., Greaves, M.J., 1982. The rare earth elements in seawater. Nature 296, 214–219.
Fan, B.J., Mei, Q.L., Wang, X.J., Meng, Y., Huang, Q.J., 2020. Geochemical comparison of mudstone and shale – a case study of the 7th member of Yanchang Formation in Ansai area, Ordos Basin. Oil & Gas Geology 41 (6), 1119–1128 (In Chinese with English abstract).
Gallego-Torres, D., MartÍnez-Ruiz, F., Paytan, A., Jiménez-Espejo, F.J., Ortega-Huertas, M., 2007. Pliocene-Holocene evolution of depositional conditions in the eastern Mediterranean: Role of anoxia vs. productivity at time of sapropel deposition. Palaeogeogr. Palaeoclimatol. Palaeoecol. 246 (2–4), 424–439.
Goldstein, S.J., Jaconbsen, S.B., 1988. Rare earth elements in river waters. Earth Planet. Sci. Lett. 89 (1), 35–47.
Gromet, L.P., Haskin, L.A., Korotev, R.L., Dymek, R.F., 1984. The "north American shale composite": its compilation, major and trace element characteristics. Geochim. Cosmochim. Acta 48, 2469–2482.
ten Haven, H.L., Leeuw, J.W., Rullkötter, J., Sinninghe Damsté, J.S., 1987. Restricted utility of the pristane/phytane ratio as a palaeoenvironmental indicator. Nature 330, 641–643.
He, C., Ji, L.M., Wu, Y.D., Su, A., Zhang, M.Z., 2016. Characteristics of hydrothermal sedimentation process in the Yanchang Formation, South Ordos Basin, China: evidence from element geochemistry. Sediment. Geol. 345, 33–41.
Hughes, W.B., Holba, A.G., Dzou, L.J.P., 1995. The ratios of dibenzothiophene to phenanthrene and pristane to phytane as indicators of depositional environment and lithology of petroleum source rocks. Geochim. Cosmochim. Acta 59 (17), 3581–3598.
Ingall, E.D., Bustin, R.M., Van Cappellen, P., 1993. Influence of water column anoxia on the burial and preservation of carbon and phosphorus in marine shales. Geochim. Cosmochim. Acta 57, 303–316.
Johnson Ibach, L.E., 1982. Relationship between sedimentation rate and total organic carbon content in ancient marine sediments. AAPG Bull. 66, 170–188.
Khaled, A., Li, R.X., Xi, S.L., Zhao, B.S., Wu, X.L., Yu, Q., Zhang, Y.N., Li, D.X., 2022. Paleoenvironmental conditions and organic matter enrichment of the Late Paleoproterozoic Cuizhuang Formation dark shale in the Yuncheng Basin, North China. J. Pet. Sci. Eng. 208, 109627.
Krzeszowska, E., 2019. Geochemistry of the Lublin Formation from the Lublin Coal Basin: Implications for weathering intensity, palaeoclimate and provenance. Int. J. Coal Geol. 216, 103306.
Langmann, B., Zakšek, K., Hort, M., Duggen, S., 2010. Volcanic ash as fertiliser for the surface ocean. Atmos. Chem. Phys. 10 (8), 3891–3899.
Lash, G.G., Blood, D.R., 2014. Organic matter accumulation, redox, and diagenetic history of the Marcellus Formation, southwestern Pennsylvania, Appalachian basin. Mar. Pet. Geol. 57, 244–263.
Lerman, A., 1978. Lakes: Chemistry, Geology. Physics. Springer, New York, pp. 237–289.
Li, M.J., Wang, T.G., Zhong, N.N., Zhang, W.B., Sadik, A., Li, H.B., 2013. Ternary diagram of fluorenes, dibenzothiophenes and dibenzofurans: Indicating depositional environment of crude oil source rocks. Energy Explor. Exploit. 31 (4), 569–588.
Li, Q., Wu, S.H., Xia, D.L., You, X.L., Zhang, H.M., Lu, H., 2020. Major and trace element geochemistry of the lacustrine organic-rich shales from the Upper Triassic Chang 7 Member in the southwestern Ordos Basin, China: Implications for paleoenvironment and organic matter accumulation. Mar. Pet. Geol. 111, 852–867.
Liao, S.L., Tao, C.H., Zhu, C.W., Li, H.M., Li, X.H., Liang, J., Yang, W.F., Wang, Y.J., 2019. Two episodes of sulfide mineralization at the Yuhuang-1 hydrothermal field on the Southwest Indian Ridge: Insight from Zn isotopes. Chem. Geol. 507, 54–63.
Lin, S.H., Yuan, X.J., Yang, Z., 2017. Comparative study on lacustrine shale and mudstone and its significance: a case from the 7th member of Yanchang Formation in the Ordos Basin. Oil Gas Geol. 38 (3), 517–523 (In Chinese with English abstract).
Liu, Q., Yuan, X.J., Lin, S.H., Guo, H., Cheng, D.W., 2018. Depositional environment and characteristics comparison between lacustrine mudstone and shale: a case study from the Chang 7 Member of the Yanchang Formation, Ordos Basin. Oil Gas Geol. 39 (3), 531–540 (In Chinese with English abstract).
Liu, Q.Y., Li, P., Jin, Z.Y., Sun, Y.W., Hu, G., Zhu, D.Y., Huang, Z.K., Liang, X.P., Zhang, R., Liu, J.Y., 2022. Organic-rich formation and hydrocarbon enrichment of lacustrine shale strata: a case study of Chang & Member. Sci. China Earth Sci. 52 (2), 270–290 (In Chinese with English abstract).
Luo, J.L., Li, J., Yang, B.H., Dai, Y.Q., Li, B., Han, Y.L., Wang, H.H., Du, J.L., 2007. Provenance for the Chang 6 and Chang 8 Member of the Yanchang Formation in the Xifeng area and in the periphery Ordos Basin: evidence from petrologic geochemistry. Sci. China Ser. D Earth Sci. 50, 75–90.
Makeen, Y.M., Hakimi, M.H., Abdullah, W.H., 2015. The origin, type and preservation of organic matter of the Barremian–Aptian organic-rich shales in the Muglad Basin, Southern Sudan, and their relation to paleoenvironmental and paleoclimate conditions. Mar. Pet. Geol. 65, 187–197.
Mclennan, S.M., 1989. Rare Earth elements in sedimentary rocks: influence of provenance and sedimentary processes. Rev. Mineral. Geochem. 21, 169–200.
Meclennan, S.M., 1993. Weathering and global denudation. J. Geol. 101, 295–303.
Meng, J.H., Liu, L.F., Zhang, M., Wang, Y., 2011. Indicative function of aromatic hydrocarbon in crude oil on depositional environment. J. China Univ. Min. Technol. 40 (6), 901–907 (In Chinese with English abstract).
Moldowan, J.M., Seifert, W.K., Gallegos, E.J., 1985. Relationship between petroleum composition and depositional environment of petroleum source rocks. AAPG Bull. 69, 1255–1268.
Mort, H., Jacquat, O., Adatte, T., Steinmann, P., Föllmi, K., Matera, V., Berner, Z., Stüben, D., 2007. The Cenomanian/ Turonian anoxic event at the Bonarelli Level in Italy and Spain: enhanced productivity and/ or better preservation? Cretac. Res. 28, 597–612.
Murphy, A.E., Sageman, B.B., Hollander, D.J., 2000. Black shale deposition and faunal overturn in the Devonian Appalachian basin: Clastic starvation, seasonal water-column mixing, and efficient biolimiting nutrient recycling. Paleoceanography 15 (3), 280–291.
Murray, R.W., 1994. Chemical criteria to identify the depositional environment of chert: general principles and applications. Sediment. Geol. 90 (3–4), 213–232.
Parrish, J.T., 1995. Paleogeography of C_{org}-rich rocks and the preservation versus production controversy. In: Huc, A.Y. (Ed.), Paleogeography, Paleoclimate, and Source Rocks, vol. 40. AAPG, Studies in Geology, pp. 1–20.
Pedersen, T.F., Calvert, S.E., 1990. Anoxia vs. productivity: what controls the formation of organic- carbon-rich sediments and sedimentary rocks? AAPG Bull. 74, 454–466.
Peters, K.E., Cassa, M.R., 1994. Applied source rock geochemistry. In: Magoon, L.B., Dow, W.G. (Eds.), The Petroleum System – from Source to Trap, vol. 60. AAPG Memoir, pp. 93–120.
Peters, K.E., Moldowan, C.C., 1993. The Biomarker Guide: Interpreting Molecular Fossils in Petroleum and Ancient Sediments. Prentic-Hall. Inc, Englewood Cliffs, New Jersey.
Peters, K.E., Walters, C.C., Moldowan, J.M., 2005. The Biomarker Guide: Column 2, Biomarkers and Isotopes in Petroleum Systems and Earth History, 2nd ed. Cambridge University Press, Cambridge, pp. 48–109.
Qiao, J.Q., Baniasad, A., Zieger, L., Zhang, C., Luo, Q., Littke, R., 2021. Paleo-depositional environment, origin and characteristics of organic matter of the Triassic Chang 7 Member of the Yanchang Formation throughout the mid-western part of the Ordos Basin, China. Int. J. Coal Geol. 237, 103636.
Qiu, X.W., Liu, C.Y., Mao, G.Z., Deng, Y., Wang, F.F., Wang, J.Q., 2015. Major, trace and platinum-group element geochemistry of the Upper Triassic nonmarine hot shales in the Ordos basin, Central China. Appl. Geochem. 53, 42–52.
Rao, H.M., Huang, W.G., 2017. Discussion on influencing factor of content of dissolved oxygen in water. J. Salt Sci. Chem. Industry 46 (3), 40–43 (In Chinese with English abstract).
Rona, P.A., Lowell, R.P., 1978. Hydrothermal systems at oceanic spreading centers. Geology 6 (5), 299.
Roy, D.K., Roser, B.P., 2013. Climatic control on the composition of Carboniferous – Permian Gondwana sediments, Khalaspir basin, Bangladesh. Gondwana Res. 23, 1163–1171.
Sarki Yandoka, B.M., Abdullah, W.H., Abubakar, M.B., Hakimi, M.H., Adegoke, A.K., 2015. Geochemical characterisation of Early Cretaceous lacustrine sediments of Bima Formation, Yola Sub-basin, Northern Benue Trough, NE Nigeria: Organic matter input, preservation, paleoenvironment and palaeoclimatic conditions. Mar. Pet. Geol. 61, 82–94.
Schenau, S.J., Reichart, G.J., De Lange, G.J., 2005. Phosphorus burial as a function of paleoproductivity and redox conditions in Arabian Sea sediments. Geochim. Cosmochim. Acta 69 (4), 919–931.
Schoepfer, S.D., Shen, J., Wei, H.Y., Tyson, R.V., Ingall, E., Algeo, T.J., 2016. Total organic carbon, organic phosphorus, and biogenic barium fluxes as proxies for paleomarine productivity. Earth Sci. Rev. 149, 23–52.
Shen, J.J., Wang, P.W., Chen, K.Q., Zhang, D.T., Wang, Y.N., Cai, Q.S., Meng, J.H., 2021. Relationship between volcanic activity and enrichment of shale organic matter during the Ordovician-Silurian transition in western Hubei, Southern China. Palaeogeogr. Palaeoclimatol. Palaeoecol. 577, 110551.
Shi, J., Zou, Y.R., Cai, Y.L., Zhan, Z.W., Sun, J.N., Liang, T., Peng, P.A., 2022. Organic matter enrichment of the Chang 7 member in the Ordos Basin: Insights from chemometrics and element geochemistry. Mar. Pet. Geol. 135, 105404.
Sicre, M.A., Marty, J.C., Saliot, A., Aparicio, X., Grimalt, J., Albaiges, J., 1987. Aliphatic and aromatic hydrocarbons in different sized aerosols over the Mediterranean Sea: Occurrence and origin. Atmos. Environ. 21 (10), 2247–2259.
Steiner, M., Wallis, E., Erdtmann, B.D., Zhao, Y.L., Yang, R.D., 2001. Submarine – hydrothermal exhalative ore layers in black shales from South China and associated fossils – insights into a lower Cambrian facies and bio-evolution. Palaeogeogr. Palaeoclimatol. Palaeoecol. 169, 165–191.
Trail, D., Bruce Watson, E., Tailby, N.D., 2012. Ce and Eu anomalies in zircon as proxies for the oxidation state of magmas. Geochim. Cosmochim. Acta 97, 70–87.

Tribovillard, N., Riboulleau, A., Lyons, T., Baudin, F., 2004. Enhanced trapping of molybdenum by sulfurized marine organicmatter of marine origin in Mesozoic limestones and shales. Chem. Geol. 213, 385–401.
Tribovillard, N., Algeo, T.J., Lyons, T., Riboulleau, A., 2006. Trace metals as paleoredox and paleoproductivity proxies: an undate. Chem. Geol. 232, 12–32.
Turekian, K.K., Wedepohl, K.H., 1961. Distribution of the elements in some major units of the Earth's crust. Geol. Soc. Am. Bull. 72, 175–192.
Tyson, R.V., 2001. Sedimentation rate, dilution, preservation and total organic carbon: some results of a modelling study. Org. Geochem. 32 (2), 333–339.
Tyson, R.V., Pearson, T.H., 1991. Modern and ancient continental shelf anoxia: an overview. Geol. Soc. Spec. Publ. 58, 1–24.
Wang, R.G., Li, W.H., Liao, Y.Y., Guo, Y.Q., Liu, H.W., 2013. Provenance analysis of Chang7 member of triassic Yanchang Formation in Ordos Basin. Geol. Bull. China 32, 671–684 (In Chinese with English abstract).
Wei, W., Algeo, T.J., 2020. Elemental proxies for paleosalinity analysis of ancient shales and mudrocks. Geochim. Cosmochim. Acta 287, 341–366.
Wolfe, G.V., Steinke, M., Kirst, G.O., 1997. Grazing-activated chemical defence in a unicellular marine alga. Nature 387, 894–897.
Xu, Z.J., Wang, Y., Jiang, S., Fang, C., Liu, L.F., Wu, K.J., Luo, Q., Li, X., Chen, Y.Y., 2022. Impact of input, preservation and dilution on organic matter enrichment in lacustrine rift basin: a case study of lacustrine shale in Dehui Depression of Songliao Basin, NE China. Mar. Pet. Geol. 135, 105386.
Yang, H., Dou, W.T., Liu, X.Y., Zhang, C.L., 2010. Analysis on sedimentary facies of Member 7 in Yanchang Formation of Triassic in Ordos Basin. Acta Sedimentol. Sin. 28 (2), 254–262 (In Chinese with English abstract).
Yang, J.J., 2002. Tectonic Evolution and Oil-Gas Reservoirs Distributions in Ordos Basin. Petroleum Industry, Beijing. In Chinese, pp. 36–37.
Yang, Y.T., Li, W., Ma, L., 2005. Tectonic and stratigraphic controls of hydrocarbon systems in the Ordos basin: a multicycle cratonic basin in Central China. AAPG Bull. 89 (2), 255–269.
Yu, W.H., Algeo, T.J., Du, Y.S., Maynard, B., Guo, H., Zhou, Q., Peng, T.P., Wang, P., Yuan, L.J., 2016. Genesis of Cryogenian Datangpo manganese deposit; hydrothermal influence and episodic post-glacial ventilation of Nanhua Basin, South China. Palaeogeogr. Palaeoclimatol. Palaeoecol. 459, 321–337.
Yuan, W., Liu, G.D., Stebbins, A., Xu, L.M., Niu, X.B., Luo, W.B., Li, C.Z., 2017. Reconstruction of redox conditions during deposition of organic-rich shales of the Upper Triassic Yanchang Formation, Ordos Basin, China. Palaeogeogr. Palaeoclimatol. Palaeoecol. 486, 158–170.
Yunker, M.B., Macdonald, R.W., Snowdon, L.R., Fowler, B.R., 2011. Alkane and PAH biomarkers as tracers of terrigenous organic carbon in Arctic Ocean sediments. Org. Geochem. 42, 1109–1146.
Zhang, B., Mao, Z.G., Zhang, Z.Y., Yuan, Y.L., Chen, X.L., Shi, Y.X., Liu, G.L., Shao, X.Z., 2021c. Black shale formation environment and its control on shale oil enrichment in Triassic Chang 7 Member, Ordos Basin, NW China. Pet. Explor. Dev. 48 (6), 1–10.
Zhang, K., Liu, R., Liu, Z.J., Li, B., Han, J.B., Zhao, K.G., 2020. Influence of volcanic and hydrothermal activity on organic matter enrichment in the Upper Yanchang Formation, southern Ordos Basin, Central China. Mar. Pet. Geol. 112, 104059.
Zhang, K., Liu, R., Liu, Z.J., 2021b. Sedimentary sequence evolution and organic matter accumulation characteristics of the Chang 8 – Chang 7 members in the Upper Triassic Yanchang Formation, Southwest Ordos Basin, Central China. J. Pet. Sci. Eng. 196, 107751.
Zhang, K.X., Li, X.S., Wang, Y.X., Liu, W., Yu, Y.X., Zhou, L., Feng, W.P., 2021a. Paleo-environments and organic matter enrichment in the shales of the Cambrian Niutitang and Wunitang Formations, South China: Constraints from depositional environments and geochemistry. Mar. Pet. Geol. 134, 105329.
Zhang, W.Z., Yang, H., Xia, X.Y., Xie, L.Q., Xie, G.W., 2016. Triassic chrysophyte cyst fossils discovered in the Ordos Basin, China. Geology 44, 1031–1034.
Zhang, W.Z., Yang, W.W., Xie, L.Q., 2017. Controls on organic matter accumulation in the Triassic Chang 7 lacustrine shale of the Ordos Basin, Central China. Int. J. Coal Geol. 183, 38–51.
Zhao, W.Z., Zhu, R.K., Hu, S.Y., Hou, L.H., W, S.T, 2020. Accumulation contribution differences between lacustrine organic-rich shales and mudstones and their significance in shale oil evaluation. Pet. Explor. Dev. 47 (6), 1160–1171.
Zheng, R.H., Wang, Y.F., Li, Z.P., Zhang, Z.H., Wang, G.L., Zhang, H., 2022. Differences and origins of hydrocarbon generation characteristics between mudstone and shale in the Seventh Member of the Yanchang Formation, Ordos Basin, China. Int. J. Coal Geol. 257, 104012.